BRNO UNIVERSITY OF TECHNOLOGY

VYSOKÉ UČENÍ TECHNICKÉ V BRNĚ

FACULTY OF ELECTRICAL ENGINEERING AND COMMUNICATION

FAKULTA ELEKTROTECHNIKY
A KOMUNIKAČNÍCH TECHNOLOGIÍ

DEPARTMENT OF BIOMEDICAL ENGINEERING

ÚSTAV BIOMEDICÍNSKÉHO INŽENÝRSTVÍ

X-RAY IMAGE DETECTORS FOR USING IN MICROCT SYSTEMS.

OBRAZOVÉ DETEKTORY RENTGENOVÉHO ZÁŘENÍ PRO APLIKACE V MICROCT SYSTÉMECH

MASTER'S THESIS
DIPLOMOVÁ PRÁCE

AUTHOR — **Bc. Gabriela Papajová**
AUTOR PRÁCE

SUPERVISOR — **Ing. Martin Mézl**
VEDOUCÍ PRÁCE

BRNO 2017

BRNO UNIVERSITY OF TECHNOLOGY
FACULTY OF ELECTRICAL ENGINEERING AND COMMUNICATION

Master's Thesis

Master's study field **Biomedical Engineering and Bioinformatics**
Department of Biomedical Engineering

Student: Bc. Gabriela Papajová ***ID:*** 154645
Year of study: 2 ***Academic year:*** 2016/17

TITLE OF THESIS:

X-ray Image detectors for using in microCT systems.

INSTRUCTION:

1) Study the problematic of microCT systems and detectors of X-ray. Make a patent review in this area. 2) Define typical physical parametrs of the real X-ray detectors and describe its impact on image quality. Focus on physical feasibility of the parameter´s evaluation. 3) Study and describe methods and techniques for the measuring of the X-ray detector´s parameters. Propose the additional methods for evaluation of the detectors typical for microCT systems. 4) Measure the X-ray detector parameters by using existed and proposed techniques for at least one detector. 5) Make a sruvey about commercial X-ray detectors which are suitable for microCT applications. 6) Discuss the achieved results and conclusions. This diploma thesis is produced in cooperation with FEI Czech Republic.

REFERENCE:

[1] BUSHBERG, Jerrold T. The essential physics of medical imaging. 3. vydání. Philadelphia: Wolters Kluwer Health/Lippincott Williams, 2012, 1048 s. ISBN 978-078-1780-575.
[2] EUCLID, Seeram. Computed Tomography: Physical Principles, Clinical Applications, and Quality Control. 4. Elsevier Health Sciences, 2015, 576 s. ISBN 9780323323017.

Assigment deadline: 6. 2. 2017 ***Submission deadline:*** 19.05.2017

Head of thesis: Ing. Martin Mézl
Consultant: doc. Ing. Bohumil Klíma, Ph.D.

prof. Ing. Ivo Provazník, Ph.D.
Subject Council chairman

WARNING:

The author of this Master's Thesis claims that by creating this thesis he/she did not infringe the rights of third persons and the personal and/or property rights of third persons were not subjected to derogatory treatment. The author is fully aware of the legal consequences of an infringement of provisions as per Section 11 and following of Act No 121/2000 Coll. on copyright and rights related to copyright and on amendments to some other laws (the Copyright Act) in the wording of subsequent directives including the possible criminal consequences as resulting from provisions of Part 2, Chapter VI, Article 4 of Criminal Code 40/2009 Coll.

ABSTRAKT

Diplomová práce se zabývá detektory rentgenového záření pro mikro-CT systémy. Teoretická část zahrnuje standartní typy rentgenových detektorů a požadavky na kvalitu obrazu pro výslednou 3D rekonstrukci. V závěru jsou popsány fyzikální parametry reálných detektorů a metody jejich měření a vyhodnocení.

KLÍČOVÁ SLOVA

Mikro-CT, detektory rentgenového záření, CCD, CMOS, fyzikální parametry, tomografie, scintilátor, MTF, CTF, DQE

ABSTRACT

The Diploma thesis deals with x-ray detectors for micro-CT systems. The theoretical part summarizes standard types of X-ray detectors and requirements on the image quality for the final 3D reconstruction. In the end, the physical parameters of real detectors and methods of their measurements and evaluation are described.

KEYWORDS

Micro-CT, X-ray detectors, CCD, CMOS, Physical parameters, tomography, scintillator, MTF, CTF, DQE

PAPAJOVÁ, G. *X-ray image detectors for using in microCT systems.* Diplomová práce. Brno: Vysoké učení technické v Brně, Fakulta elektrotechniky a komunikačních technologií, 2017. 71 s. Vedoucí diplomové práce Ing. Martin Mézl.

PROHLÁŠENÍ

Prohlašuji, že svoji diplomovou práci na téma *X-ray image detectors for using in microCT systems* jsem vypracovala samostatně pod vedením vedoucího semestrálního projektu a s použitím odborné literatury a dalších informačních zdrojů, které jsou všechny citovány v práci a uvedeny v seznamu literatury na konci práce.

Jako autor uvedené diplomové práce dále prohlašuji, že v souvislosti s vytvořením této práce jsem neporušila autorská práva třetích osob, zejména jsem nezasáhla nedovoleným způsobem do cizích autorských práv osobnostních nebo majetkových a jsem si plně vědoma následků porušení ustanovení § 11 a následujících zákona č. 121/2000 Sb., o právu autorském, o právech souvisejících s právem autorským a o změně některých zákonů (autorský zákon), ve znění pozdějších předpisů, včetně možných trestněprávních důsledků vyplývajících z ustanovení části druhé, hlavy VI. díl 4 Trestního zákoníku č. 40/2009 Sb.

V Brně dne ....

(podpis autora)

PODĚKOVÁNÍ

Děkuji vedoucímu diplomové práce Ing. Mézlovi za účinnou, metodickou, pedagogickou odbornou pomoc a další cenné rady při zpracování mé diplomové práce. Chtěla bych také poděkovat doc. Ing. Bohumilu Klímovi Ph.D. za jeho podporu, trpělivost, rady, inspiraci a diskuze při vypracování této diplomové práce.

V Brně dne ……..….. ……

(podpis autora)

TABLE OF CONTENT

LIST OF FIGURES

INTRODUCTION

The computed tomography (CT) method serves for the internal structure examination of spatial objects. These non-destructive methods use the x-ray radiation for acquiring a set of projections of the object. Next, these data are processed in the computer reconstruction algorithms to obtain the internal structure images of the examined object. These output data are most often available in a form of a set of spatially parallel slices of the object.

The most known usage of the CT systems is in the medical field with a usual resolution slightly under 1mm. However, not only medical CT systems are being developed. For the high resolution applications, micro-CT systems development is nowadays increasing in many fields beside the medical. These areas include structural material analysis, archeology, electronics, food industry, oil and gas industry, geology etc.

Micro-CT manufacturers make efforts to improve the resolution, image quality and user friendliness, and to shorten the time to image data output. The x-ray detector is one of the most important parts in micro-CT systems. This diploma thesis deals with these detectors. It summarizes the theory around X-ray detectors and physical principles used. Based on this theory a suitable detector for micro-CT applications can be found. Detectors image parameters and their measuring methods are described in next part.

The practical part of the thesis is a description and proposal of measurement methods for the evaluation of a various X-ray imaging detectors. The ultimate goal is to evaluate physical parameters and functional properties of the X-ray detector for microtomography and to find a suitable selection strategy. In other words, the goal is to find the most suitable combination of real detector parameters for a micro-CT system based on "*resolution at the distance*" principle.

Final measurements will be accomplished in cooperation with former FEI Company (Thermo Fisher Scientific) on HeliScan microCT.

1 PRINCIPLES OF MICROCT SYSTEMS AND X-RAY DETECTORS

1.1 History

The first micro tomographic system had been developed by Jim Elliot at the beginning of 1980s. 3D images of 50µm small tropical snail were reconstructed first time. The micro-CT scans of bones had been obtained already in 1994 thanks to this nondestructive method providing 3D images of scanned object. MicroCT technique had opened a field with a new application for non-destructive testing such as detecting grain faults at the micro level (cracks, inclusions, defects in materials, bone growths). [1]

An example of an advanced microCT system is HeliScan which was developed by cooperation of former FEI Company and Australian National University (ANU), see Figure 1.

Figure 1: Micro-CT system - FEI Company (source: www.fei.com)

1.2 Computed tomography

Obtaining of 3D slices of an examined object using computed tomography requires two basics steps – *a projections acquisition* and a *3D reconstruction*. The projections acquisition is being performed on CT scanners. Scanned data are being processed in computer systems in the next

phase to obtain 3D slices. A various visualization techniques can be understood as optional post processing steps [16].

1.2.1 CT scanner configuration

The first necessary action in CT is to acquire the complete dataset of 2-dimensinal projections in 360 °. Various configurations of micro-CT scanners are known, depending on the purpose of the scanner or on the development history and patents (depends which company is an originator). Figure 2 shows one of the basic hardware configurations of microCT scanner. It contains a static detector and a static X-ray source. The sample is being fixed on the rotating stage between the X- ray source and the detector. The geometric magnification is reached by a cone-beam emitted from a point source, passing through the sample and hitting the detector. The ratio of the detector plane distance to sample stage rotating axes distance from the emitting spot defines the geometric magnification. The principle is known as "magnification/resolution at the distance". [8]

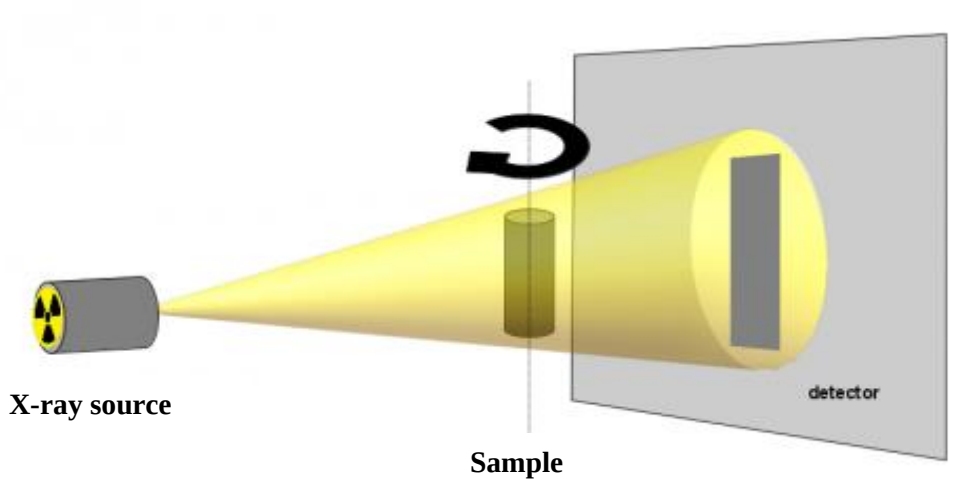

Figure 2: Micro-CT system principle [19]

1.2.2 X-ray imaging physical essentials

The basic physics principle of the X-ray imaging technique is an interaction of X-ray with matter. The main mechanism of the interaction is called the photoelectric effect.

The photoelectric effect attenuates the photons. The attenuation is proportional to the cube of the atomic number of the elements and inversely proportional to the cube of the photon energy. It means that the dependency is not only on the material of the scanned sample, but also on the energy spectrum of the X-ray source. When the X-ray beam penetrates the sample, there is an exponential attenuation dependence on the material and on the traveled distance. The material constant is energy dependent. It appears in the exponent of the attenuation formula and is called

“linear attenuation coefficient”. The coefficient expresses the amount of radiation which is attenuated at infinitely small depth in the material. Total attenuation reflects the sum of all the local linear attenuations along the X-ray beam. Therefore, X-ray projections (or the X-ray image) is the sum of all local attenuations along the X-ray beam.

The attenuation of the radiation by the object is determined for a large number of paths through the object slice by means of a measurement arrangement consisting of an X-ray tube and a radiation detector system. The radiation intensity at the detector is recorded at a fixed predetermined intervals which is called *the exposure time*.

A lot of projections are demanded in CT for 3D slice calculation. Those projections are acquired using various kinds of trajectories and are slightly turned by a very small angle (1°).

The reconstruction method assumes the sample slice divided into small volume elements. The elements have a square base and are called voxels. A constant X-ray attenuation is assumed in each individual voxel.

While an X-ray interacts with the material, following types of interaction are distinguished, see Figure 3.

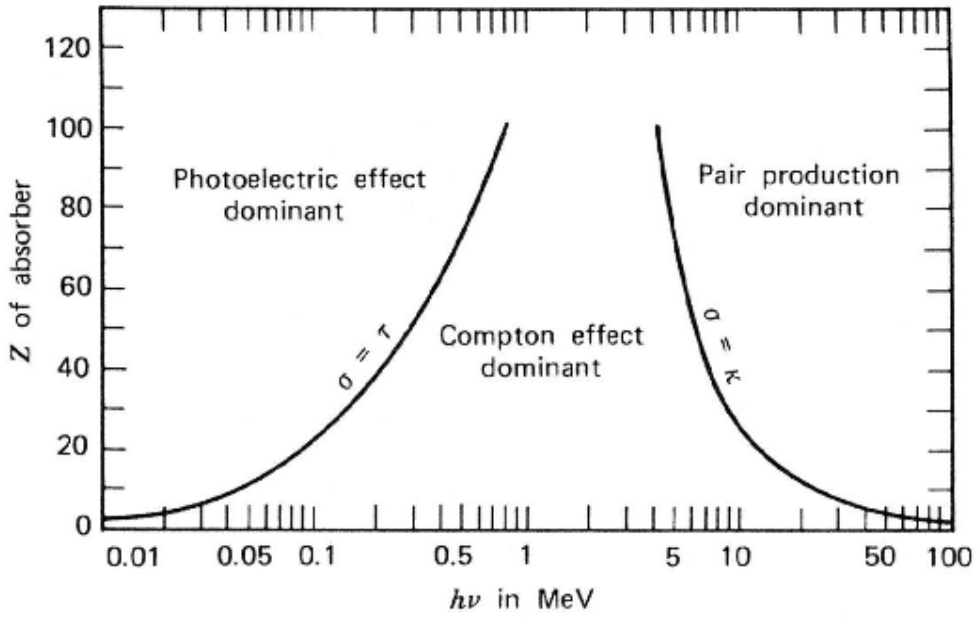

Figure 3: Three major types of x-ray interactions are determined by the absorber atomic number (Z) and the photon energy (hv) [9].

Compton scattering is the interaction of photons with free or weakly bound electrons. Part of the photon energy is used for electron to escape from the atom and the rest of the energy is emitted in the form of less energetic photon. If the photon passes only a part of his energy to the electron which is weakly bound on the outside orbital of the atom, here is scattered electron and photon of lower energy are created. Scattered electron further ionizes and excites electron orbitals and thus causes a formation of secondary and tertiary scattered electrons. The photon

loses its energy to recombine with other atoms and the photoelectric effect ceases. During the Compton scattering the number of photons does not change, the photons only deflect from the original direction and lose part of their energy and increase theirs wavelength. [10]

The X-ray photon is completely absorbed in the photoelectric interaction the by transferring all of its energy to an electron. On the other hand, photons change both directions and energy in the Compton scattering as well. [11]

Pair Production appears only when x-ray photon energies are sufficiently high. This redundant energy is used for the electron-positron pair creation, but it lost immediately by excitations and ionizations of other atoms around.

1.2.3 Attenuation of the radiation

The probability of each phenomenon mentioned previously depends on the radiation energy (E). The total attenuation in the sample combines all of these phenomena, because the x-ray sources usually generate wide spectrum of energies. The attenuation depends on the object material. A certain amount of photons is being removed from the x-ray beam on their path through the object. The linear attenuation coefficient of material μ (ρ, Z, E) is a complex function of the sample density, and of the atomic number (Z) which varies because of the Radiation energy (E) change.

Lambert-Beer's Law

The x-ray attenuation in the matter depends on the direction of the x-ray, so if the x-ray penetrates through the sample so the Lambert-Beer's Law for monochromatic beam is defined as:

$$I = I_0 e^{-\mu L} \tag{1.2}$$

Where I is the penetrated Intensity, I_0 is the Intensity of the entering beam, μ is the attenuation coefficient and L is the sample length [12] [53].

1.2.4 Anode voltage and current settings

X-ray tomograms with high spatial resolution require a cone x-ray source with sufficient angle to cover detector dimensions [25]. Anode voltage and tube current setting is a task which assures a proper exposure achievement. Simply said, the aim is to record as many details in the sample as possible (a largest possible gray scale in the projection is desired) without saturating any part of the detector, including detector parts which are not covered by the sample.

The radiation energy range and its intensity must be set according to the sample material and its thickness. The radiation energy range depends on the sample thickness and its material. The anode voltage defines the upper energy limit of the radiation spectrum. It is possible to crop the lower limit of energy spectrum by using filters. The low energy radiation can be eliminated using a metal filter on x-ray source. The cropping energy range depends on the filter material, and the attenuation depends on the filter thickness. Different materials used for X-ray beam

filtering are illustrated in Figure 4.

Figure 4: Commonly used materials for the energy spectrum filtering [53]

The tube current has to be set to achieve a sufficient intensity of radiation for sufficient exposure. The exposure is given by the product of the radiation intensity hitting the detector and the exposure time. This fact allows a variation of those two parameters. However, the scanning time minimization requirement leads to the use of an exposure time which is as low as possible.

1.2.5 Sample resolution in micro-CT

The resolution of a μ-CT scanner depends on the system geometry. The size of an elementary sample which can by projected on a single pixel at the detector with given system geometry can be assumed as theoretical resolution. The influence of different spot sizes is shown in Figure 5. During the image magnification, smaller spot size provides sharper and clear image. [30]

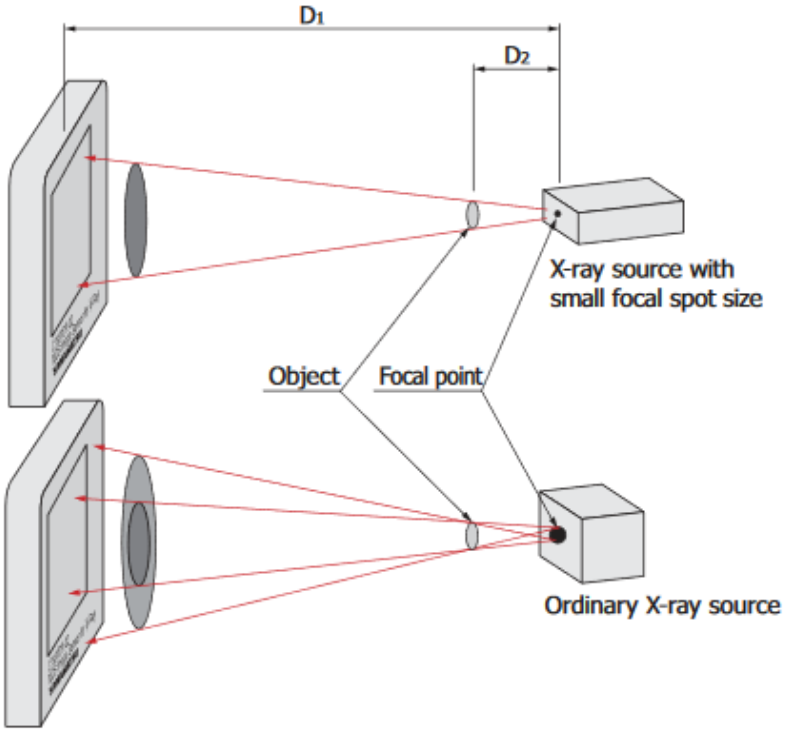

Figure 5: Influence of a different spot size on image distortion [26]

Figure 6 shows the system geometry which is used for the resolution definition of the micro-CT system in equations 1.3 and 1.4. [16]

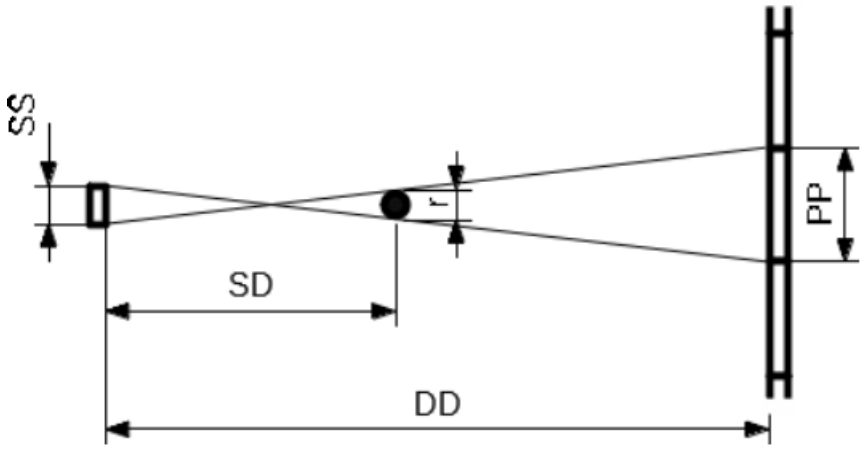

Figure 6: System geometry for the resolution definition

$$r = PP\frac{SD}{DD} + SS\frac{DD - SD}{DD};\ SS \neq 0, \tag{1.3}$$

$$r_{ss0} = PP\frac{SD}{DD}; SS = 0, \tag{1.4}$$

Where the system geometry parameters are:

PP - detector pixel pitch

DD - detector distance

SD - sample distance

SS - spot size

r - resolution

Example: PP = 139 µm; SS = 1.5 µm; DD = 330 mm; SD = 2 mm

r = 2.34 µm; r_{ss0}=0.84 µm

It is clear, that the spot size of an X-ray beam limits the resolution of an image. Finite spot size of the X-ray source is required, so the heat can be drained off the target. The heat is produced by the electrons hitting the target. X-ray flux is limited by the small spot size and high energy. The focal spot is expected to grow with the increasing X-ray flux. [24]

1.3 Projections acquisition

The radiation passing the specimen and hitting the detector is recorded at fixed predetermined time intervals which are called *exposure time* or *exposure period*. Detector pixels records the number of x-ray photons hitting them during the exposure period. The number of photons is converted to the charge and then digitalized by an A/D converter in the detector. The matrix of these converted numbers create a digital gray-scale image typical for X-ray imaging techniques. The conversion chain principle will be described in more details later. It is essential for the understanding of functions and parameters of a real x-ray detector.

Each individual image is called a projection in CT. A set of projections needs to be acquired for sample a 3D sample image reconstruction angularly shifted usually by a constant angle step. However, CT techniques use many kinds of trajectories, not only the rotary/circular one. The step size is determined by desired image resolution, typically less than 0.1°.

1.3.1 Scanning time

The number of projections and exposure time define the scanning time. Scanning time depends on desired resolution, which determines the angular step and number of projections per rotation. The other aspects are the sample height to be scanned, a chosen trajectory and the number of full rotations around the sample axis. The exposure time depends on the sample size and material. Chosen trajectory can be helical (single or double) or circular. [31]

The image averaging also makes the scanning time few times longer. The image averaging is ordinarily used to increase the signal to noise ratio of image detector. A detector with a high SNR can reduce the scanning time.

Table 1 shows different samples such as Edwards Brown Limestone (EBL) or grindstone

and their scan settings.

Table 1: Example of different scanning times for selected samples in HeliScan microCT

Diameter / Sample	*4mm EBL*	*4mm EBL*	*2mm EBL*	*2mm EBL*	*3mm grindstone Dremel*	*3mm grindstone Dremel*
Type of trajectory	helical	double helical	double helical	helical	helical	circular
Exposure time [s]	0.35	0.35	1.4	1.2	0.4	0.43
Nr. of accumulations	7	6	5	5	4	6
Sample height [mm]	14.5	7	4.65	6.2	9.5	-
Voxel size [µm]	2.065	2.077	1.268	0.892	1.2636	1.2636
Acquisition duration [hours]	**~ 6**	**~ 4**	**~ 33,5**	**~ 13,5**	**~ 12**	**~ 4**

1.4 Reconstruction of CT data

1.4.1 Iterative reconstruction

An iterative reconstruction technique was used in the first commercial CT system in history. Iterative image reconstruction is, from the mathematical point of view, a procedure, where many individual steps ("iterations") are made with trial and error method. It starts with a very rough structure estimation of the examined object and iterates to the final image that most closely matches the measured values of the cumulative absorption coefficients from different angle projections.

The first CT systems operated with a simple form of statistical IR called Algebraist reconstructive technique – ART [3]. Figure 7 briefly explains the principle of iterative reconstruction. Underlined values represent the total absorption coefficient of various projections which are acquired after the scan though the absorption coefficients for each pixel are still unknown. The algorithm gradually specifies (in the direction of the long arrow) the absorption coefficients (grey values) for each pixel which compares the measured values from different directions and intermediate results for each pixel in steps are refined until the output (matrix on the top) is identical to the original.

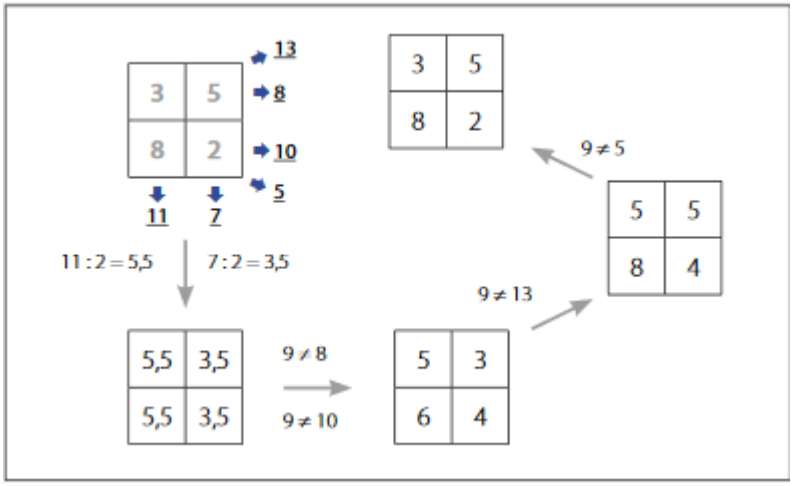

Figure 7: Principle of iterative reconstruction, simplified for a 2 × 2 image matrix. [2]

One of the biggest advantages of an iterative algorithm is that the increasing number of iterations in the image ensures the result closer to the original, but also effectively reduces the image noise. On the other hand, too many iterations can blemished the final reconstruction image and the main disadvantage of the IR is longer reconstruction time and enormous demands on computing power. [2] The reconstruction time was significantly lowered in case of the FEI optimized iterative algorithm for the efficiency reason.

1.4.2 Filtered back projection

Huge time demands on the reconstruction were the reason why the iterative CT image reconstruction was replaced by analytical methods called Filtered Back Projection (FBP). Significantly less demands for computing power and also easier implementation caused that FBP became the gold standard in the CT image reconstruction. [4]

In 1917, Johann Karl Radon described how to express an object using a set of projections. The mathematical operation is called “Radon transform” after the author. Then, Radon proved that the inverse formula of the transform exists - "Inverse Radon Transform".

The first step is to collect endless individual projections from different angles during a rotation around the object and then reflected them back together to an approximate picture of the object, where a visible attenuation of X-ray on internal structures of scanned object appears.

The FBP algorithm is demonstrated in Figure 8. A visible star artifact is caused by the approximation of values from the polar coordinate system to the square coordinate system. The visibility of mentioned artifact can be also caused by small amount of projections. Ideally, the Radon Transformation is defined for the continuous signal - an infinite number of angles of rotation and an infinite number of shifts.

Figure 8.A shows absorption coefficients from individual angle projections which are represented by the column height. Picture 8.B shows the acquired data back projected. Picture

8.C demonstrates the visibility of the star artifact. RAMP filters are usually applied in frequency domain for the star artifact reduction.

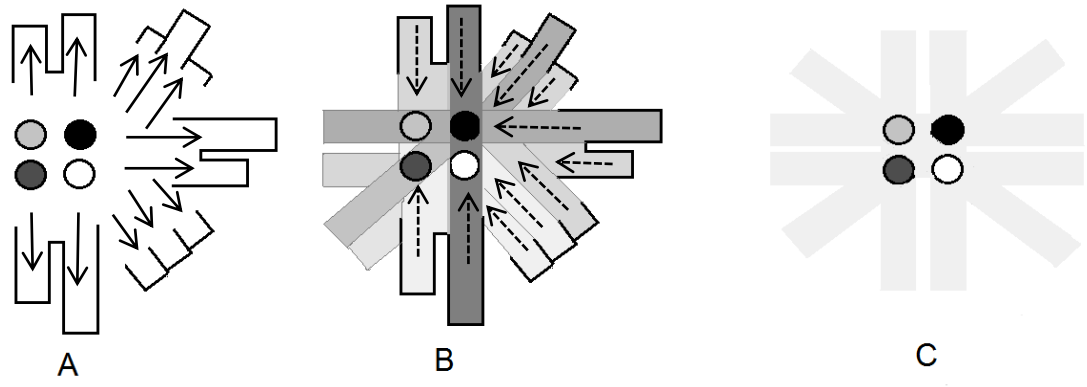

Figure 8: Principle of a simple back projection [2]

From the mathematical point of view, the main disadvantage of the FBP algorithm is the requirement of a very accurate set and low noise projections.

1.4.3 Calibration of images before reconstruction

Dark Field image (DF)

The purpose of acquiring a dark field image during the scan is the subtraction of dark current offset (more in CCD detectors). The dark current increases with the temperature growing, depending on the chip architecture. In order to reduce electronics offsets in the image, the dark frame must be acquired with the same exposure time and temperature as projections. The dark field image also compensates a detector errors.

Clear Field image (CF)

There are two reasons for a clear field image acquisition. The first one is that the intensity of the X-ray source is not homogeneous over the detector area. The radiating characteristic is not spherical and the distance from a spot to individual pixels of the flat panel detector is not the same. The intensity of a clear field image decreases from the center to edges/corners of the detector. Clear Field images are acquired to be used for compensate the non-uniformity of the X-ray intensity. Basically, the projection images are divided by the clear field images into corresponding pixels. [27]

1.4.4 Artifacts

There exists few parasitic phenomena in the CT, which can degrade the final image quality. The main causes are usually data inconsistency in the image, undersampling, high dense material,

sample movement, noise, fault detector calibrations or incorrect CT scan parameter settings. Many artifact causes can be compensated in reconstruction algorithms in modern CTs. The most often causes are the following:

Beam Hardening

X-ray photons emitted from the x-ray source have a wide spectrum of energies. Photons with the lower energy are decelerating with the higher probability while the x-rays are passing through the object. The energy spectrum behind the sample spectrum is moved toward the higher energies. Soft X-rays need to be filtered to reduce the beam hardening artifacts in images.

From the image point of view, the beam hardening effect causes false information about the object density. [9, 13] An example of the beam hardening influence in shown Figure 9.

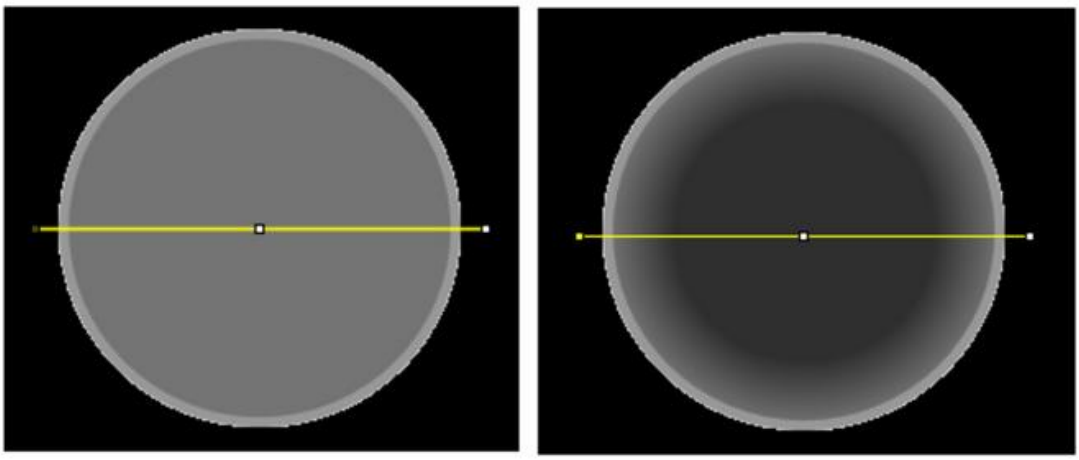

Figure 9: Beam hardening artefacts in a cross-section of the sample on the right picture. [19]

Edge artifacts

Double edges and streaks are caused by specimen shifts between the first and last projections or by a shift from the center of rotation which appears during the projections acquisition. [18] An example of these artifacts is shown on the left part of Figure 10.

Ring artifacts

Ring artifacts are caused by different detection efficiency or sensitivity of some x-ray detector pixels. It causes permanent erroneous reading at each angular position during circular trajectory. This type of artifact is more visible on uniform sample [9, 17]. Example of ring artifact is shown in Figure 10 on the right.

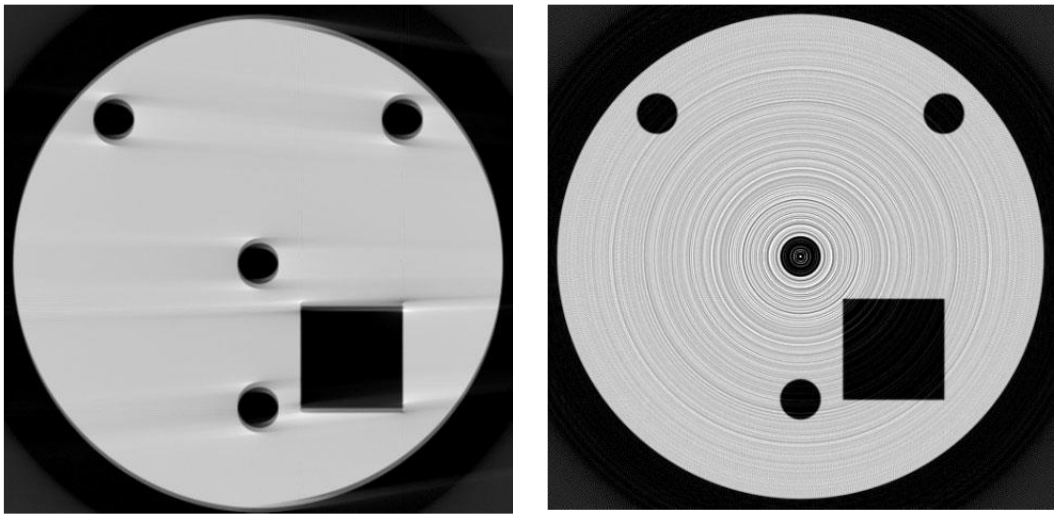

Figure 10: *Left*: Double edges and streaking, *right*: Ring artifacts [18]

Slice thickness

Thicker slices decrease a contrast resolution in the image and cause different types of artifacts, e.g. partial volume artifacts. Thinner slices allow increasing of spatial resolution but also highlight the noise**.**

1.5 X-ray sources

X-rays can be generated either by hitting the accelerated electrons on a target, or by changing the trajectory of electrons by synchrotron.

1.5.1 Microfocus X-ray sources

X-ray tubes operate on the basic principle of electron beams. Free electrons are generated by incandescent tungsten cathode in vacuum and accelerated by an electric field which is generated by a voltage in the range from tens - hundreds kV. These electrons hit the metal surface of the target (anode). The X-rays energy range depends on the voltage between the cathode and anode and also depends on target material.

Microfocus X-ray sources are based on the same principle as a classic tubes but they are constructed differently. Electron beam is centered by magnetic lenses and focused on the target with a diameter of a micron. The spot size is influenced by the current through lenses coils. Thus the X-ray is generated only by the spot area, where the electrons hit the target. The spot area diameter is called spot size. The maximum voltage according to the type of the tube is between 90 kV and 450 kV in real X-ray sources.

X-ray tubes are divided by the target into reflection and transmission types as is shown in Figure 11. Reflection target X-ray sources produce bigger heat dissipation. For transmission targets x-rays go thought, therefore the scattering effect is less significant than in the reflection target. Smaller spot size can be achieved in transmission X-ray sources. The important thing is that the resolution is influenced by the spot size, hence for higher resolution transmission are targets preferred [33].

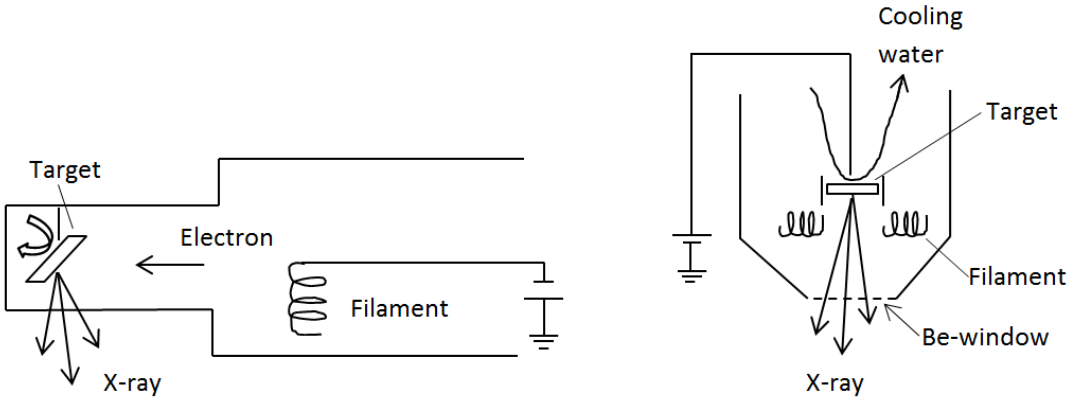

Figure 11: Structure of X-ray tubes: reflection target (left) and transmission target (right)

X-ray tubes are available in open and closed form. Closed tubes are hermetically closed and have permanent vacuum, they are pumped once upon being manufactured. Closed types are usually suitable for lower voltages under 100 kV.

X-ray tubes with spot size under 1 micrometer require higher voltages so open systems are preferred. Vacuum is created by a separate vacuum pump during the operation in open tubes. This solution is more complex and expensive and needs more maintenance

In general, X-ray tubes have a low efficiency. Relatively large amount of dissipating heat energy needs to be removed from the tube with a suitable liquid cooling system [31, 32].

1.5.2 Synchrotron radiation X-ray sources

Electromagnetic radiation is formed upon the interaction of accelerated electrons with the magnetic field. The direction of the charged particles changes and particles emit photons. Thus electrons are moving in accumulation ring and are accelerated by the magnetic field. Emitted X- ray moves in a direction of tangent to the curved trajectory of electrons in the accumulation ring. In comparison with microfocus x-ray source, synchrotron creates a monochromatic radiation, spatial coherence and provides possibility of a phase contrast imaging. [34]

1.6 X-ray spectrum

The X-ray spectrum is composed of the Bremsstrahlung and the characteristic radiation. X-ray

spectrum can be described relatively to the number of photons in the spectrum or the transmittance of an X-ray beam can be evaluated. The X-ray beam is influenced by the current and the voltage of an X-ray tube, the filtration and the material from which the target is made. View on a Hamamatsu X-ray source tungsten-diamond target is shown in Figure 12.

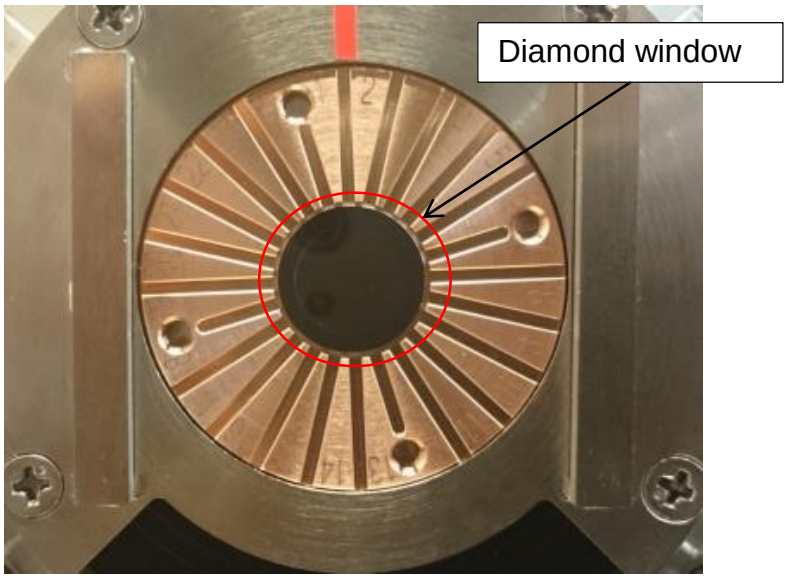

Figure 12: Transmission type of a diamond window with a tungsten target

Target

The energy of photons of the Bremsstrahlung radiation is proportional to the atomic number of the target material. This means that higher atomic number increases the amount of braking radiation photons. The energy of photons of characteristic radiation is also affected. Example of the X-ray spectrum on 100kV is in Figure 13.

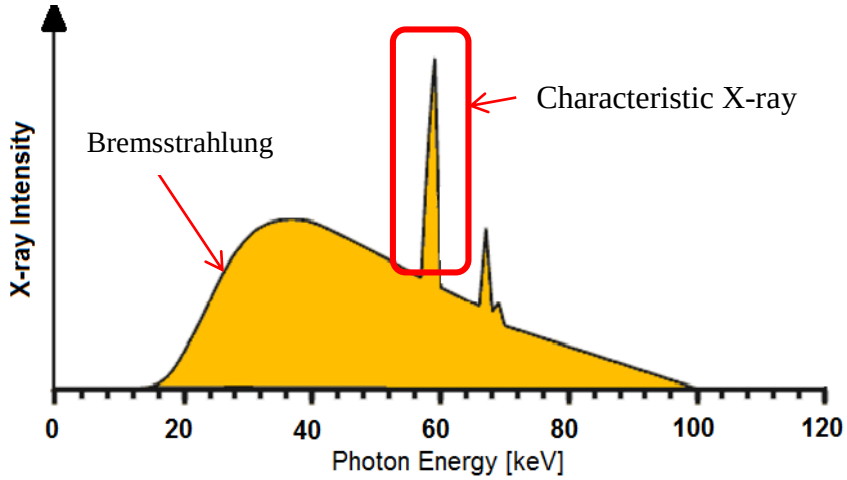

Figure 13: Example of the X-ray spectrum on 100kV with a Tungsten target.

Exposure time

Basically, a certain quantum of x-ray photons is demanded for reaching the high quality X-ray image. The quantum is proportional to the product of the target current and the exposure time. The exposure time affects the total acquisition time, therefore as low as possible exposure time is desirable to be set [42].

Tube Voltage

Tube Voltage indicates the maximum energy that can be present in the Bremsstrahlung radiation spectrum. The amount of radiation is approximately proportional to the second power of the tube voltage.

Tube Current

It expresses the amount of electrons that are accelerated towards the target (Anode) where they interact.

Spectrum Filtration

Additional gun filtration is useful for low-energy photons removing. As said in section 1.4.4., low energy photons can cause beam hardening artifacts.

1.7 Types of detectors

X-ray detectors principles can be divided into two main groups according to the method of detection.

The first detectors type uses *direct detection* of X-ray which is converted into electrical signal. The hitting x-ray photons create electron-hole pairs in a pixel chip. The voltage of this charge is then converted to a digital number.

In addition, during the indirect detection, the x-ray is transformed into visible light using the scintillator layer which covers the image sensor surface. The visible light hits a standard CCD or CMOS image sensor and is converted onto image data.

1.7.1 Direct conversion

Image detector of this type implements a conversion of an X-ray signal into an electric signal in one step. The conversion of the X-ray to electric signal - electron-hole pairs – uses the internal photoelectric absorption. The most often used converter material is amorphous selenium [6]. The number of electrons generated by direct X-ray detection is *proportional to the energy* of the incident photons. The advantage of the semiconductor detector is the large signal and accurate pulse location. This results in high conversion efficiency and high absorption of the incident radiation [43]. An issue is that X-ray can damage the electronics inside the detector and therefore indirect detection needs a protection against them. Appropriate lens or fiber optics systems need to be used for that reason.

Basic principle of direct conversion is shown in Figure 14.

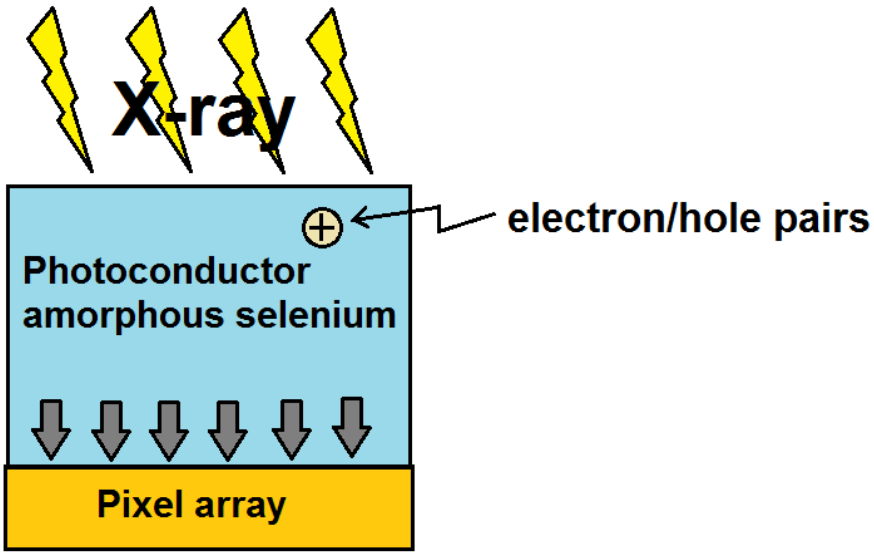

Figure 14: Detector with direct conversion layer of amorphous Selenium [23]

1.7.2 Indirect conversion

Indirect conversion detectors are used more often in micro-CT systems. The detection is based on a two-step conversion. The first step is the X-ray conversion into a visible light using the phenomenon of fluorescence – a latent X-ray image is transformed into the light intermediate image. The light intermediate image is converted by 2D array of photodiodes (amorphous silicon *a-Si*) or a charge-coupled CCD structure of an image detector to an electrical signal in the second step. Examples of indirect conversion configurations are shown in Figure 15.

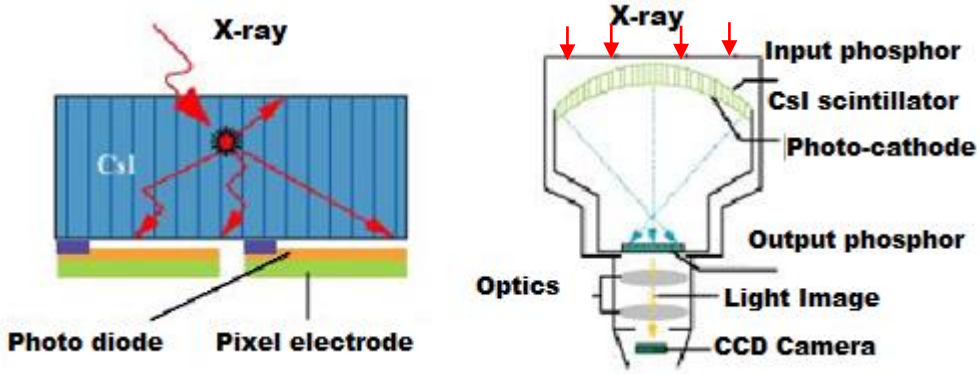

Figure 15: Principles of detectors with indirect conversion [23]

1.7.3 Flat-panel detectors

Flat panels belong to semiconductor detectors and provide signals for direct digital conversion of an X-ray image. Flat panel contains a lot of small elements, called pixels which create an image

matrix. The most common is a combination of a CCD or a CMOS detector with a scintillation layer. In general, flat panels have better spatial and contrast resolution in comparison with other types. Flat panels with direct conversion are based on amorphous selenium and works without a scintillator, thus photons interact straight with semiconductor detector and the created electric charge is converted directly into an electrical signal. The mentioned type of detector with direct conversion is used less often than the detector with the indirect conversion.

In both types of detector the electrical signal is registered by a special matrix of transistors which are implemented in an integrated circuit.

1.7.4 Scintillators

The principle of scintillation detectors of ionizing radiation is based on materials which can absorb quantum of ionizing radiation and react by generating flashing lights.

The most commonly used materials are crystals of sodium iodide activated by thallium - NaI (Tl), Cesium Iodide (CsI), Gadox (GOS) or phosphor for detection purposes.

Figure 16 schematically shows the basic principle of twosparkle different kinds of scintillators. Each x-ray photon, absorbed within the scintillating layer, generates a sparkle of visible light (scintillation) that is detected by high efficient CCD or CMOS sensors which are described later.

In general, Phosphor scintillator manufacturing is easier and provides higher light gain (better efficiency). On the other side the light scattering and lower resolution are not convenient.

Thin CsI crystals can improve the resolution but their manufacturing is complex and expensive. An important parameter for scintillator materials is the absorption coefficient. A large absorption coefficient is typical for a CsI crystal due to the internal structure. A crystal of CsI has a needle structure which decreases scattering and increases spatial resolution in comparison with the diffusion scintillator, see Figure 16 [5, 43].

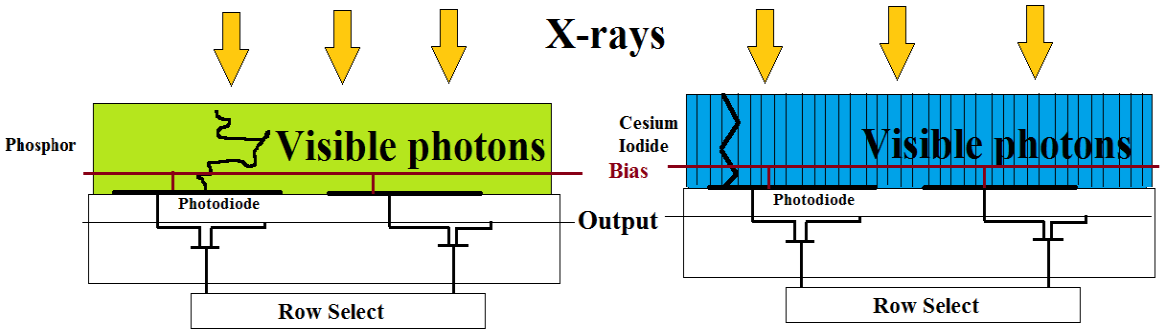

Figure 16: Principle of fluorescence screens, left: diffused phosphor layer, right: structured CsI layer [5]

Detector resolution is given by the pixel pitch but thicker scintillator layers definitely

decrease spatial resolution however the quantum efficiency is higher. Typical dependence of scintillation layer thickness on contrast transfer function and on light output (~ detective quantum efficiency) is shown in Figure 17.

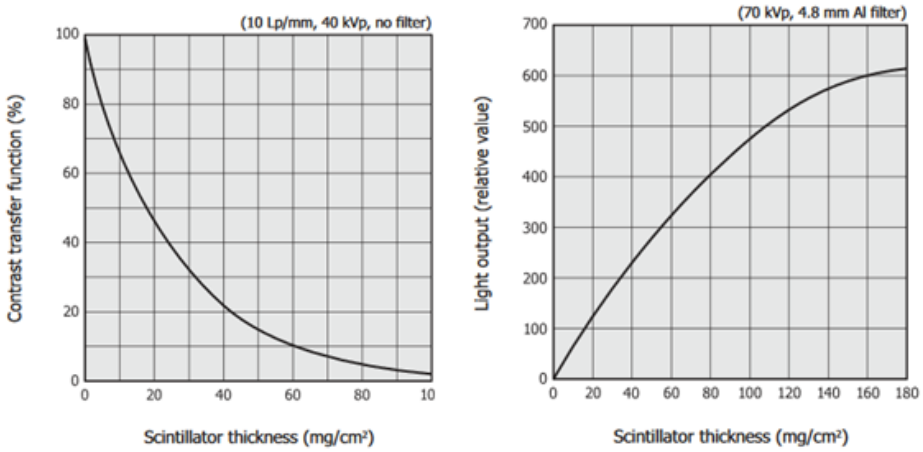

Figure 17: Influence of scintillator thickness (CsI) on resolution and on light output [26]

For a flat panel detector construction following dependencies can be postulated:

Scintillator

- Low scintillator thickness causes low DQE and increases the required dose and exposure time
- High scintillator thickness makes higher scattering and lower resolution.

Radiation energy and dose

- The scintillator material is energy dependent, each material is suitable for a different energy spectrum, see Figure 18.

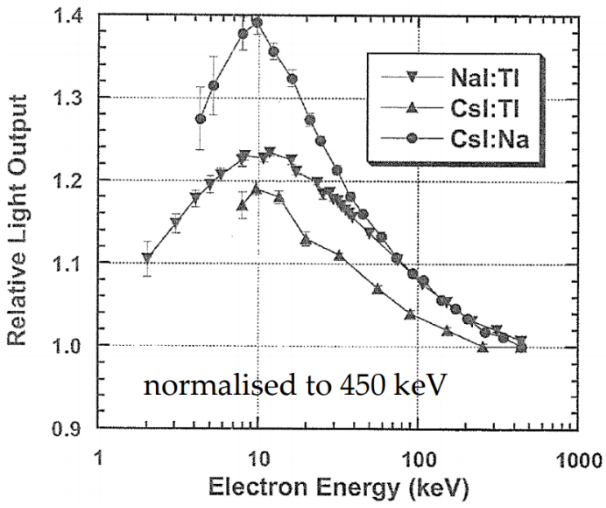

Figure 18: Scintillator material light output vs. radiation energy dependence [50]

- Small dose leads to long exposure time and vice versa.

Temperature

- Scintillator material efficiency is strongly dependent on temperature, see Figure 19.

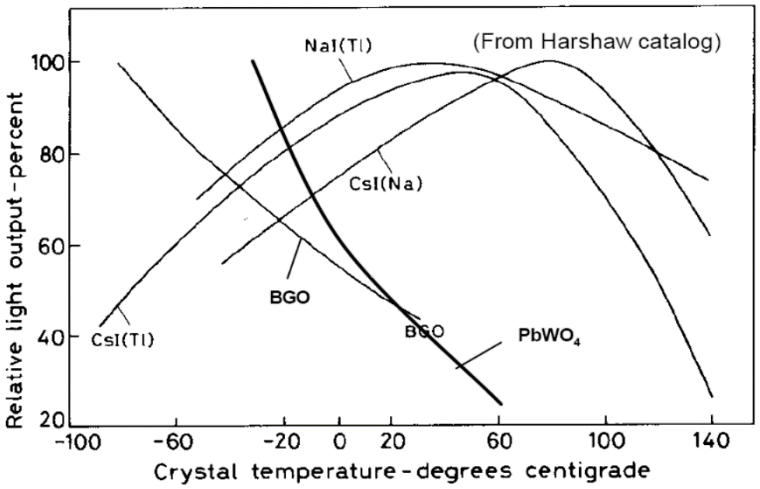

Figure 19: Relative light output of scintillator material vs. temperature [50]

Pixel photodiode and photodiode 2D array

- Small pixel size causes smaller light sensitivity and vice versa.
- Small pixel pitch causes high scattering and vice versa.
- Small pixel pitch allows high resolution.
- Small pixel photodiode capacitance increases sensitivity to visible light and shortens the exposure time
- Small pixel photodiode capacitance increases the noise and vice versa.

A lot of construction dependencies affects transfer parameters of the detector and its suitability for certain CT scanners. The flat panel detector construction is always a compromise for a particular field of use. Finally detector parameters significantly affect the construction of the CT scanner. Primarily, the detector distance and pixel pitch directly affect the resolution of the scanner, as is explained in section 1.2.5.

1.7.5 CCD image sensors

Charge Coupled Devices were invented by Willard S. Boyle and George E. Smith in 1969. CCD usage was conceived as an experimental computer memory but their ability to convert light into an electrical signal made them the best known light detectors.

Incident light generates an electrical charge in the semiconductor. Electrons cannot be freely moved on the chip due to vertical negative potential walls which repel the electrons. The system of horizontal negative electrodes formed on the chip creates a grid of "potential wells" from which electrons cannot escape.

The CCD chip is basically a shift register which is exposed to the light. The CCD chip has several layers – the most important is the layer of silicon and a layer of SiO_2, impermeable for electrons, see Figure 20. Potential wells which were mentioned in the previous paragraph, are actually pixels that collect electrons. The amount of pixels is a very important parameter. During the interaction between photons of light and the semiconductor, photons transmit their energy which causes that semiconductor generates electrons which are kept on the same place because of the positive charged electrode.

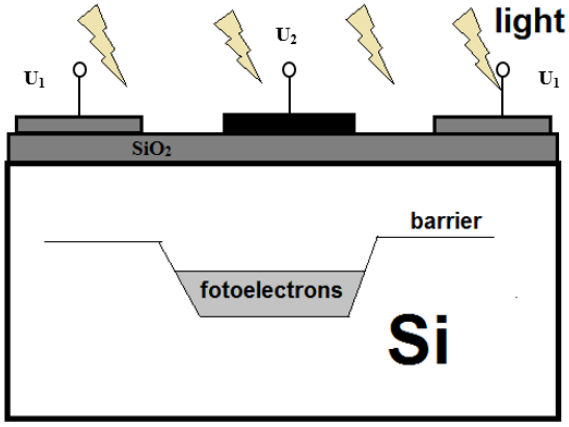

Figure 20: Cross-section of the CCD chip

CCDs are used in combination with scintillators, which convert X-rays to visible light for obtaining high quality images. Another feature which is used in CCD detectors with scintillator is a fiber optics plate (FOP) that protects CCD chips against the X-ray and helps to increase the resolution [26, 35].

1.7.6 CMOS image sensors

The electronics is integrated in the sensor cell which has its own amplifier and is directly addressed and read (unlike the CCD, which is read sequentially). Because the electronics area occupies part of the cell and reduces the sensitive part of the cell so micro-objectives are used to concentrate more light on this part. This feature compensates the image noise which is created by necessary high gain due to the small area of the sensitive cells.

CMOS sensors operate on the principle of photodiodes which measure current at the time of readout. This fact increases the sensitivity of detection. The readout can be in any sequence, for example only an area of interest can be read thanks to direct addressing. Detection area and processor are on one chip together. Figure 21 shows a typical CMOS active sensor pixel with microlens, photodiode and transistors.

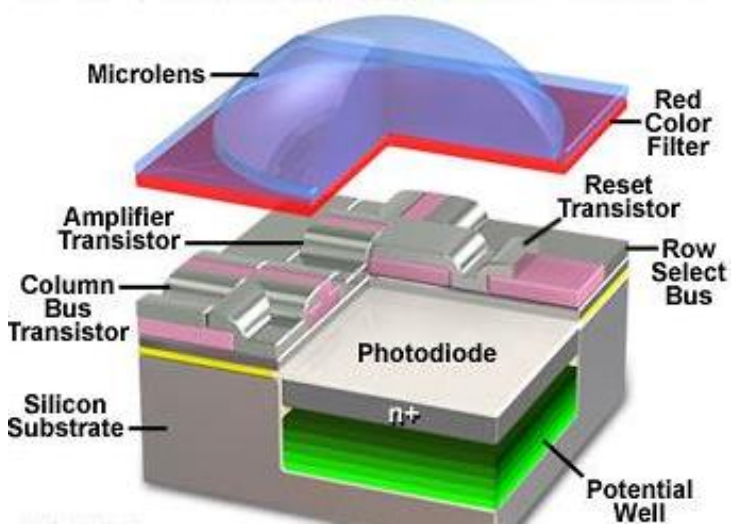

Figure 21: CMOS: Anatomy of one active pixel sensor photodiode [31]

The advantage of CMOS detectors is that charges are integrated simultaneously in all pixels and provide higher Signal to Noise Ratio and also Detective Quantum Efficiency (DQE). Also the production is cheaper in comparison with a CCD [35, 47].

1.7.7 Binning

Binning feature allows combining charges from multiple pixels in the CCD hardware. This function basically improves the signal to noise ratio and lowers the resolution (increase effective pixel pitch) of the detector. Detector without binning takes a signal of each pixel in the image, whereas detector with the binning 2x2 takes the sum of each matrix of 2x2 pixels. That way, the signal is four times bigger compared to the image without the binning but the resolution is cut on a half. Binning allows charges from neighboring CCD pixels to be combined so the readout speed become faster.

2 X-RAY DETECTORS PARAMETERS

The main goal of x-ray detection is an objective measurement of a quantum of energy, intensity and other characteristics of an X-ray. Completely precise measurements are theoretical assumption only X-ray measuring process is affected by a number of adverse physical and technical factors in real systems. Limiting and distorting factors of x-ray detection will be described in the following section.

Following chapters contain definitions of basic parameters considered in X-ray imaging detectors.

2.1 Detection efficiency

As it was mentioned before the main purpose of radiometric detection is an objective measurement of the radiation intensity or the quantum of energy in a specific location.

The quantum of energy registered by the detector on the output is always smaller (often even much smaller) than the number of a quantum of energy which really passess through the detector.

2.1.1 DQE (Detective Quantum Efficiency)

DQE describes how effectively x-ray photons are used to create an image. It basically describes the efficiency of a detector itself under ideal conditions and preserving the SNR. Therefore, it contains the information about the presence of noise and sharpness in the image and determines what can be visible in an image. On the contrary, DQE does not inform us about the contrast in the image. It is expressed in percentage. The following equation shows how can DQE can be determined [6]:

$$DQE = \frac{G^2 q\, MTF^2}{NNPS^2} \qquad [\%]\,, \tag{2.1}$$

where G is the system gain; q is the mean incident fluency; MTF is the Modulation Transfer Function; and NNPS is the normalized Noise Power Spectrum which is related to the large area signal [48].

2.2 Time resolution and dead time

The fact that each energy quantum is coming to the detector in discrete non-regular time intervals is necessary to be taken into account. When the intensity of the radiation is increasing, particles are coming with smaller and smaller time intervals. Due to this fact, the detector has a finite time

resolution.

Another time delay exists between the moment when the energy quantum interacts with a sensitive detector layer and the moment of an electric pulse at the detector output. This time delay is caused by physical processes in the detector itself. Among these processes we can include diffusion of electrons and ions in the material of the detector, the charge collection electrodes, the time period of deexcitation, the duration of the scintillation, etc. Different detectors have various time responses depending on the detector type, sensitive area size, material and structural construction.

Next delays can be found in the analogue electronics including photodiodes discharging times, the analog amplification and the data A/D conversion. Sequential digital processing of the data in detector electronics and data readout from the detector introduces another delay.

2.2.1 Time resolution

Time resolution is a time that detector needs to process and register the response signal from one quantum of energy.

2.2.2 Dead time

Detector *dead time* is a time interval between the detection of a single quantum during which the detector is not able to correctly detect other quantum. During this time, the detector is insensitive to radiation or the second response signal would be composed as a first.

The dead time of the detector causes that some quantum of energy that arrive in a "too quick succession" is not detected. This leads to reducing the detection efficiency, whereby (and this is the worst case) the detective efficiency is not constant, but is dependent on the intensity of the analyzed radiation - arises nonlinearity response. This can lead to significant errors in measurement procedures. [7]

2.2.3 Frame rate

Detector *frame rate* describes the maximal frequency of continuously acquired images. The frame rate is an inverted value of the minimal detector exposure time. The frame rate can significantly affect the total scan time in many cases in CT systems, when enough radiation intensity and minimal exposure time can be used [28].

2.3 Detector basic transfer parameters

The output of the detector AD converter to dose can be described by following pictures for individual pixels of the detector. Ideally, we expect an AD output proportional to the dose as shown in Figure 22-A. The maximal output value of the A/D converter is assumed to be the Y_0

value. The whole processing chain before the AD converter in the range of 0 and Y_0 output values is desirable to be linear in the ideal case.

However, many factors as the background radiation, the scintillator to CCD chip join non-uniformity, the photodiode nonlinear response to photons count, the amplifier nonlinearity and the x-ray source non-uniformity of course causes output response shown in Figure 22-C. An individual response characteristic exists for each detector pixel.

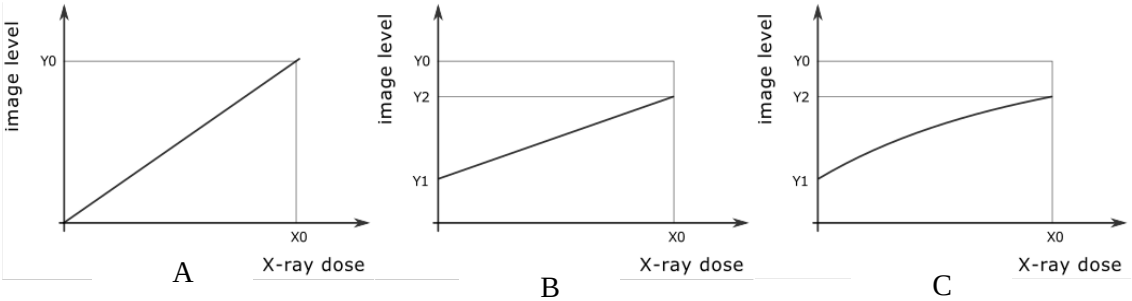

Figure 22: X-ray detection dose to output transfer characteristics: A – Ideal, B – Linear, C – nonlinear

2.3.1 Gain

Detector gain is defined as a ratio of the converted digital value of pixel to number of x-ray photons hitting the pixel. The gain knowledge helps to rescale image signals into units of the used X-ray flux. [28]. The ideal gain value is usually assumed for the whole detector gain according to Figure 22-A.

The real response of the detector approaches courses in Figure 22-B or C. The offset and gain calibration is performed in detector digital electronics as the image post processing. The offset and gain calibration maps are implemented as images in the detector electronic or computer driver, so we have calibration data for each pixel individually. The gain calibration can be done in a number of ways, but the basic idea is that raw image data from ad converter are rescaled in the way to approach the ideal output characteristic in Figure 22-A.

The whole offset in the detector pixels (Y_1 value in Figure 22) is called dark current. Offset data are subtracted from AD converter raw data. By this operation, the Y_1 point is shifted to zero.

The real gain can be rescaled by preprocessing the raw data by offset multiplying or by dividing by gain calibration data in case of compensation according to picture 22B. In case of more precision gain calibration can be partwise calibration performed. Multiple gain calibration data files are required in this case

2.3.2 Signal to noise ratio (SNR)

Like any kind of signal processing field describing the signal to noise ratio (SNR) as an amount

of useful information in the signal, the image processing in the x-ray detection systems has the same approach. The signal represents the spatial intensity of the image between the displayed object and surrounding. The noise represents disturbing statistical fluctuations in the image. The image quality is given by the SNR (signal to noise ratio) parameter.

The SNR can be defined as ratio of the mean image intensity I_m to its standard deviation *N* and is expressed in decibels [22]:

$$SNR = 20 \log\left(\frac{I_m}{N}\right) \qquad \text{[dB]} \qquad (2.2)$$

It means that the SNR does not depend only on the detector properties, but also on the detector settings, a type of the sample etc. The SNR is a signal parameter, not detector parameter. However, the detector introduces a noise into the signal in the whole signal processing chain until the A/D converter: the scintillation, light to electric signal conversion, electric signal amplification and A/D conversion.

2.3.3 Dynamic range

Dynamic range is the specified interval of acceptable values for the measurement. This interval is determined by the sensitivity threshold and by the maximum value of the scanned quantity. The meaning of dynamic range in imaging system is represented by gray scale. Theoretically, the amount of gray scale levels is given by the bits depth of the A/D converter. The logarithmic value of dynamic range is expressed:

$$DR = 20 \log(Y_0) \qquad \text{[dB]} \qquad (2.3)$$

Detector dynamic range is usually affected by its output characteristics. Ideally AD converter uses full range of its output levels. In a real situation, the AD converter output moves in the range between Y_1 and Y_2 values as shown in Figure 22-B, C, because its input is limited by an offset and a real gain. Precisely, the dynamic range of the detector is given by the detector pixel, which has the lowest difference $Y_2 - Y_1$.

$$DR = 20 \log(Y_2 - Y_1) \qquad \text{[dB]} \qquad (2.4)$$

Even if a gain calibration is applied as post-processing, it doesn't improve the dynamic range. It doesn't increase the number of output levels of the detector pixel.

2.3.4 Linearity

Linearity can be understood as an unchanged pixel output response to the same energy quanta striking the pixel. Many complex interactions run inside the detector pixel structure and the final response involves photons and electrons of different energies. If the output signal is not proportional to the particles energy, then the same quantum of energy has a different output response, according to the distribution of the total energy between secondary particles with different energies.

2.4 Spatial image quality parameters

2.4.1 Modulation Transfer Function (MTF)

Modulation Transfer Function describes how the spatial frequencies are transmitted from the object to the final image. It describes the distortion of the image with using a specific imaging system.

It is defined as a ratio of output image contrast in the image plane to input object contrast in the object plane of the imaging system [48]

2.4.2 Line Spread Function (LSF)

The LSF describes the response of the imaging system to a line light source in the spatial domain. It describes the most sharp line profile which can be identified in the image. It is expressed as a function of one variable which is perpendicular to the line source.

2.4.3 Spatial resolution

There are many definitions of the spatial resolution. Generally, it is defined as an ability to see or distinguish spatial separated details without blurring. In the field of imaging systems, the spatial resolution is defined as a capability to transfer spatial information from an object into image. It is expressed in line pairs per mm [lp/mm].

We defined theoretical resolution for micro CT system in chapter 1.2.5. It assumes, that some object is distinguished by one pixel of the detector. This definition serves for micro-CT system design purposes and spot size impact consideration in a micro-CT system. It assumes the ideal ability of the detector to distinguish details in the picture. This definition is affected by real resolution of the detector.

2.4.4 Contrast to Noise Ratio (CNR)

The image quality is defined as the ratio of contrast to noise (contrast-to-noise ratio, CNR). For a constant value of the CNR, a certain amount of photons, which is determined by current, is required.

$$CNR = \frac{p_s - p_b}{\sqrt{\frac{STD(s^2) + STD(b^2)}{2}}} \tag{2.5}$$

Where $\boldsymbol{p_s}$ is average pixel value of the signal, $\boldsymbol{p_b}$ is average pixel value of the background, $\boldsymbol{s}$ is the signal and $\boldsymbol{b}$ is the background. [48]

2.5 Target parameters for micro-CT systems

2.5.1 Geometry

We will focus onto devices with geometrical magnification only, in which the resolution increases with the distance between the sample and the detector. Unfortunately, the increased geometrical magnification can result into blurriness, depending on the X-ray source spot size. Some other micro-CT devices use microscope objectives to make the x-ray beam parallel and also to increase the magnification and the resolution.

To create a three-dimensional image the whole data set of two-dimensional projections needs to be obtained. The source and the detector are in fixed position and the object is mounted in the sample holder and rotates around the vertical axis. In principle, the x-ray source should be able to focus the electrons in a very small spot size on the target. CCD cameras detectors with scintillator layer are used most often.

In devices micro-CT X-ray tube and detector are static, while the sample rotate around a vertical or horizontal axis. The movement of the sample may result in live specimens or non-fixed damage and artifacts. Magnification is reached either by scanning the beam in a cone shape or optical equipment located before the impact of parallel X-ray detector. These devices allow zooming, but they are limited by the size of the scanned sample. The 2D images can be also obtained using the micro CT scanners. Two types of the X-ray micro-CT scanners configuration are shown in Figure 23. The left image shows the micro-CT scanner configuration with a conical shape X-ray beam which directly magnifies the sample. The second image on the right shows the configuration of the micro CT scanner with the parallel x-rays where the magnification is achieved with the optics, located in front of the detector.

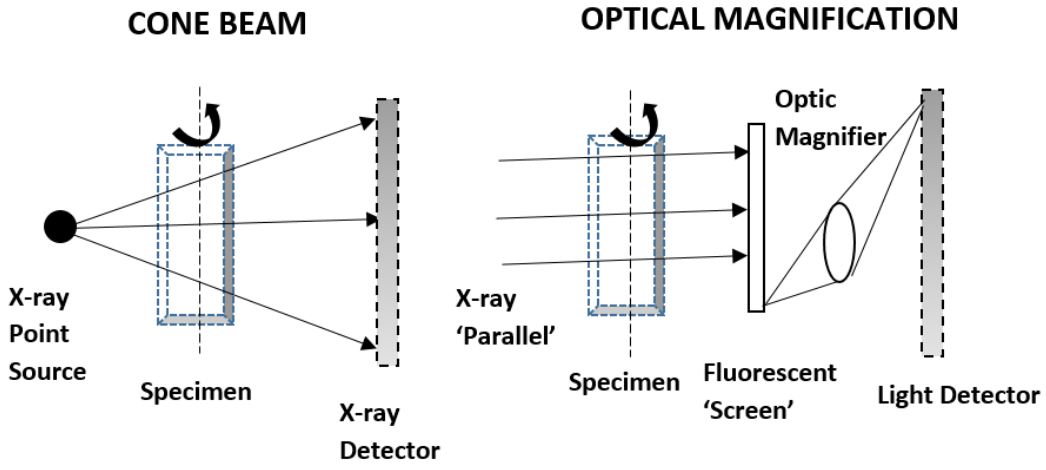

Figure 23: Two types of geometry in micro-CT systems. [14]

2.5.2 Exposure time and frame averaging

Increasing the exposure time for each projection and increasing the number repeated (averaged) projections are the most common techniques to achieve higher signal to noise ratio.

Exposure time and tube current are set in such a way that the pixels values are close to the maximal value of the detector AD converter. The maximal SNR can be achieved by this settings for single projection. Those methods also bring some limitations, for example higher dose or longer exposure time can easily saturate the detector.

On the other hand, frame averaging multiplies n-times the signal and so *random noise* is being averaged. Frame averaging decreases the noise but also increases the total scan time as well as the higher exposure time.

2.5.3 Pixel size and resolution

Resolution

Image resolution is the most relevant parameter for any detector of x-rays. The image resolution or resolving power can be determined as the ability to separate two placed signals with respect to the Rayleigh criterion.

Pixel size

Larger pixel size is suitable to increase the dynamic range and signal to noise ratio (SNR) but this option is in opposite with the requirement of smaller pixel size for better resolution.
Finding a compromise between the dynamic range, the SNR, pixel size and the MTF to obtain an "optimal" combination of parameters is the goal of the micro-CT scanner design.

A critical effect is the light scattering in the scintillator layer. Its thickness cause decreasing the spacial resolution because the light is scattered across many pixels around. [15]

The important parameters for systems with geometrical resolution are the spot size, pixel size, the sample distance and detector distance as was shown in chapter 1.2.5.

3 X-RAY DETECTOR PARAMETERS MEASUREMENT

3.1 Method of spatial resolution measurement

We can find number of definitions and number of parameters for the image detector spatial resolution. This section discusses these parameter definitions and measurement methods.

The Point Spread Function (PSF) describes the profile in the imaging system which is caused by point light source and complete information about the spatial resolution. A simpler way to determine the PSF is to measure the Full-Width-at-Half-Maximum (FWHM) in the acquired edge profile image, see example in figure 24-a. FWHM is in that case equal to 1.

The Fourier transform of the PSF is used more often do describe the image system resolution. The frequency response is called Modulation Transfer Function (MTF) and it is shown in figure 24-b. The definition of the MTF is in chapter 2.4.1.

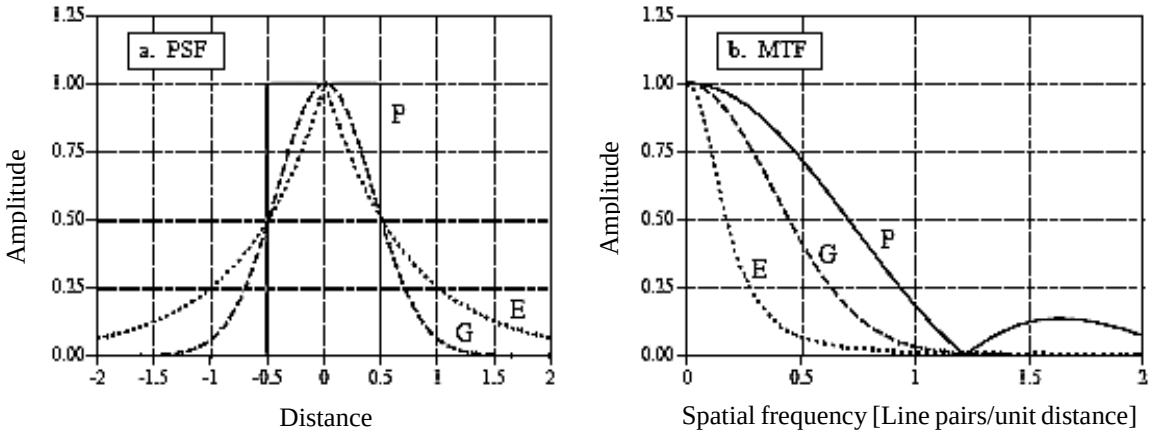

(a.) **(b.)**

Figure 24: (a): Examples of PSFs, (b): Examples of MTFs [20]

To measure the imaging system resolution the line pair pattern, which has black and white stripes is used. The resolution is taken as the spatial frequency where the stripes become indistinguishable. An example of a line pair variable pattern is in Figure 25. The typical measured profiles in the pattern image are shown at the right side of Figure 25 for different frequencies. The MTF is normalized by the peak to peak responses of line pairs in the image in function of the spatial frequency. As a distinguishable line frequency is considered a value for which the MTF reaches 0.1 [20, 29].

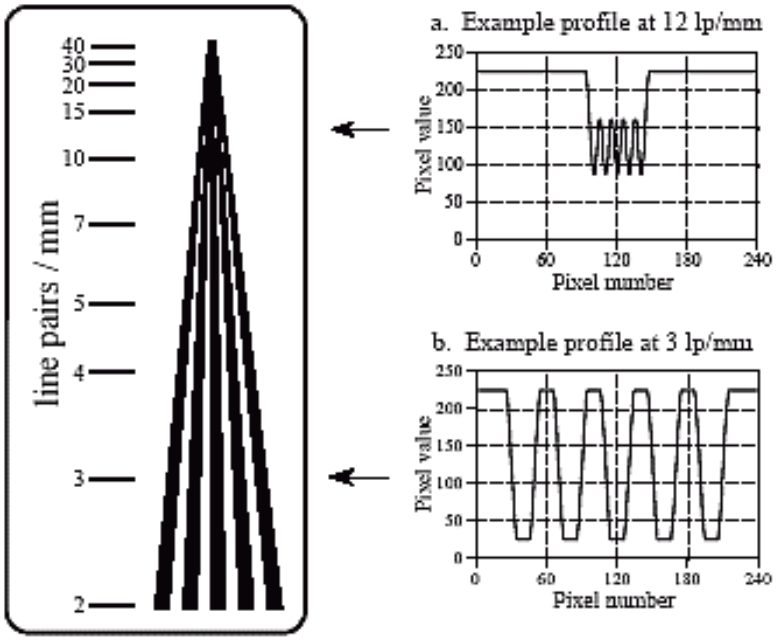

Figure 25: Line pairs gauge and profiles example [20]

Another method to get the Line Spread Function (LSF) and the edge response is calculating them from the acquired edge profile. The first step is to acquire the edge response and crop it within 10 - 90 % range. The second step is the numeric derivation of the profile. We get the LSF as a function of a pixel number. It is necessary to multiply it by the pixel pitch of the detector if we want to consider the resolution in millimeters.

3.2 Method of SNR measurement

Generally, many methods of measuring Signal to Noise Ratio (SNR) were published. An experimental method is based on finding the standard deviation around the maximum value in the image in homogeneous sample. This measurement cannot be precise because it is almost impossible to find such precisely homogeneous sample [21].

3.3 Calculation of Dead time readout

Dead time of the electronics readout can be calculated as a difference between the integration time and the real exposure time. The mentioned parameters can be obtained from the user's manual.

3.4 Linearity characterization

Detector linearity is an important requirement. The linearity of most detectors is about 99%.

The following linearity measurement method uses an aluminum step-wedge with few steps about 50 μm thick located on the detector. A homogeneous beam needs to be used. The entire detector area around the step-wedge needs to be covered with led foils.

To compensate the irregular intensity level of X-ray beam and dark current of electronics is needed to acquire dark field and clear field image as mentioned in chapter 1.3. The cross section of the acquired image is plotted with the logarithmic scale for better presentation of the non-linear effect. Ideally, the line crosses all vertexes of edges as shown in Figure 26.

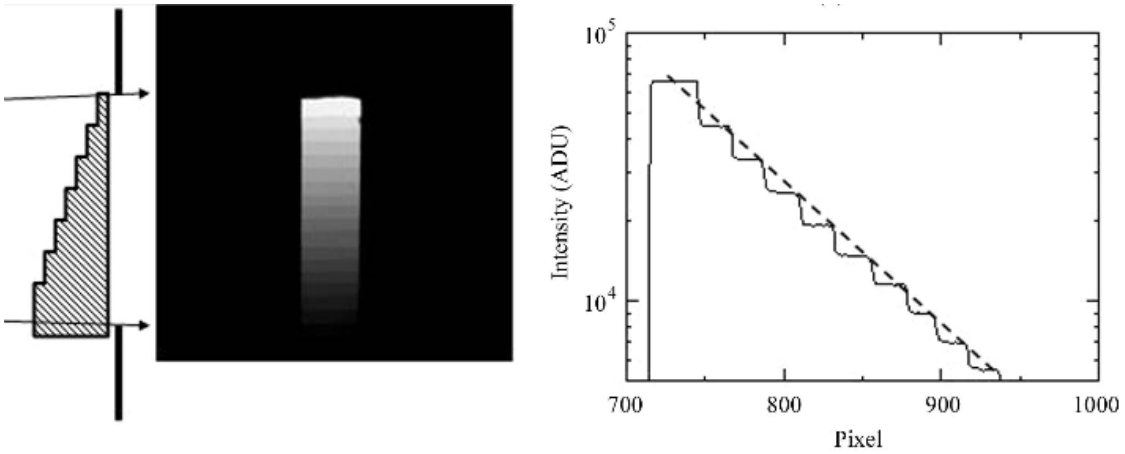

Figure 26: Image of aluminum step-wedge on the left and example of measured linearity of CCD detector on the right [28]

This method is quite simple for implementation however the results can be affected with many errors due to various beam intensity, saturation of detector or pixel inhomogeneity. [28]

3.5 Method of dynamic range measurement

Dynamic range is measured according to input signal levels and it is a very important parameter of a detector.

The dynamic range can be measured in the following order: Using homogeneous X-ray source flat field image needs to be acquired with exposure settings just before the detector saturation. The exposure setting needs to be set tentatively. Median gray value can be taken as the maximum image level I_{Xmax} in Figure 27. The dark field image needs to be taken in the next step. Its median value is the I_0 value in the picture. S_{0min} is division of the AD converter. It is usually 1 for the integer AD converter output. Now we can calculate the dynamic range according to the equation 3.1.

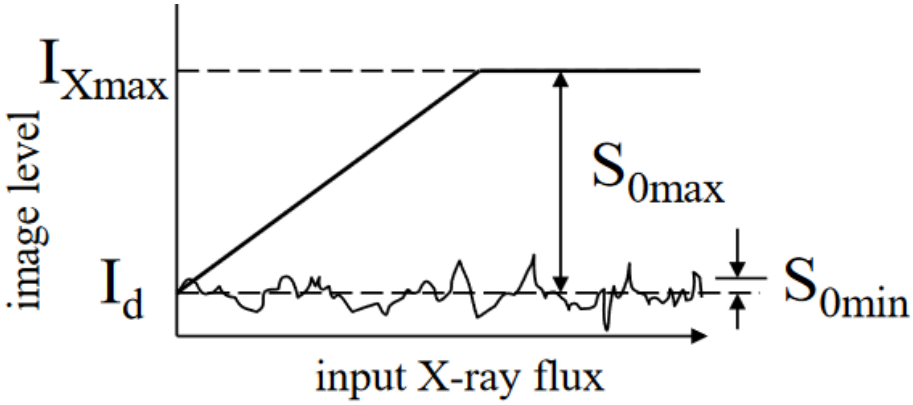

Figure 27: Dynamic range [28]

$$DR = 20 \log\left(\frac{S_{0max}}{S_{0min}}\right) \quad \text{[dB]} \quad (3.1)$$

where S_{0max} is the maximum signal range. It can be calculated as $S_{0max} = I_{Xmax} - I_d$. S_{0min} is the minimum signal level [28, 36, 43].

4 MEASUREMENT OF DETECTOR CHARACTERISTICS

Detector characteristics and their measurement techniques were explained in previous chapters. The parameters and measurement of concrete detector will be discussed in this chapter. The detector is used in the FEI Company Heliscan micro-CT scanner.

4.1 Varian/Varex PaxScan 4343CB

4.1.1 Catalogue parameters

The detector which is used in the microCT system is defined as an amorphous silicon flat panel detector (FPDs) for X-ray imaging. Total pixel area of the detector is 42.7 cm of height and 42.7 cm of width and the pixel size of a receptor is 139 μm.

Image Quality parameters are listed in Tab. 2:

Table 2: Image quality parameters according to the Product Description [37]

Image quality parameters	Value
MTF (1x1) at 1 lp/mm	54%
DQE (1x1, quantum-limited)	74%
Contrast Ratio (Small Area -10 mm):	< 7%
Dynamic Range	94 dB
Energy Range	40 - 150 kVp
A/D Conversion	16-bits

4.1.2 Signal conversion steps

In case of the flat panel detector by Varian, X-rays are absorbed in the Cesium Iodide scintillator. It converts X-ray into light with a wavelength around 550 nm. Varian states that the quantum efficiency at mentioned wavelength is about 80%. Light intensity depends on the energy of the X-ray photons.

Emitted photons of light are caught by photodiodes of a pixel array. Another step is electron/hole pairs conversion which creates voltage accumulated in the photodiodes capacitance. The voltage signal is converted by the Analog – Digital Converter (ADC) into a digital form

and saved in the corresponding address in the image matrix inside the Command Processor Unit. [37]

The whole signal conversion chain is described in the block diagram in the Figure 28.

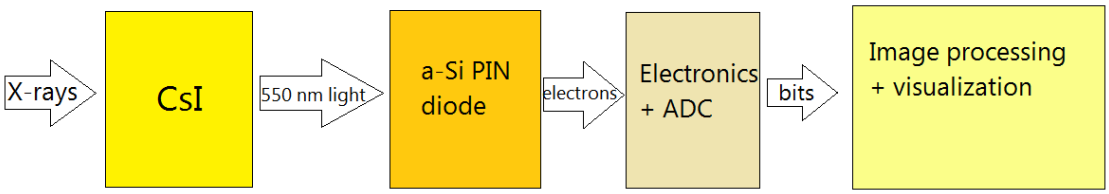

Figure 28: Signal conversion steps in the detector

The individual pixel non-linearity was described in chapter 2.3. There was said, that pixels of the detector do not have the same transfer response. This detector attribute can be demonstrated by the dark field AD converter raw image shown in Figure 29. A non-uniform pattern corresponding to manufacturing process print is visible in the image. Defective pixels are the whitest or very dark. Noisy pixels, too high gain pixels, and pixels with insufficient response with too low gain are taken as defective. The offset, gain and defective pixels map correction can be performed in the command processor of the detector. Calibration procedures are semi-automated in this detector. The detector command processor performs gain and offset calibration according to the following formula [52]:

$$image_{data} = \left(\frac{raw_{image\_data} - offset_{data}}{gain_{data} - offset_{data}} \right) \quad (4.1)$$

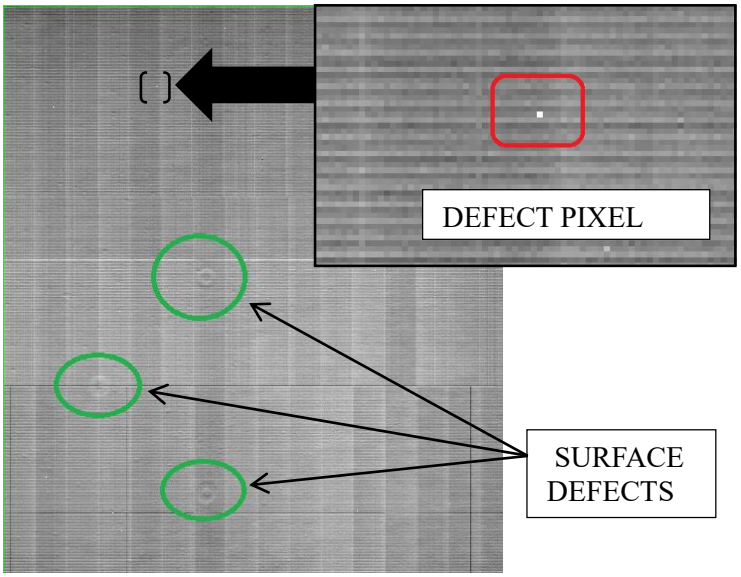

Figure 29: Dark Field Image with corrections turned off

4.1.3 Offset Calibration

The offset calibration (dark current calibration) can be done by subtracting the dark field image from each raw image data taken by the detector.

An example of the offset calibration file example for the detector model PaxScan 4343CB is shown in Figure 30. The mean pixel value is 3034 and the standard deviation value is 88. It means that the maximal Y_1 value defined in Figure 22 for the 4343CB detector can be assumed as a sum of these numbers, so its value is 3122. In relation to the AD converter range it is 4.8 %.

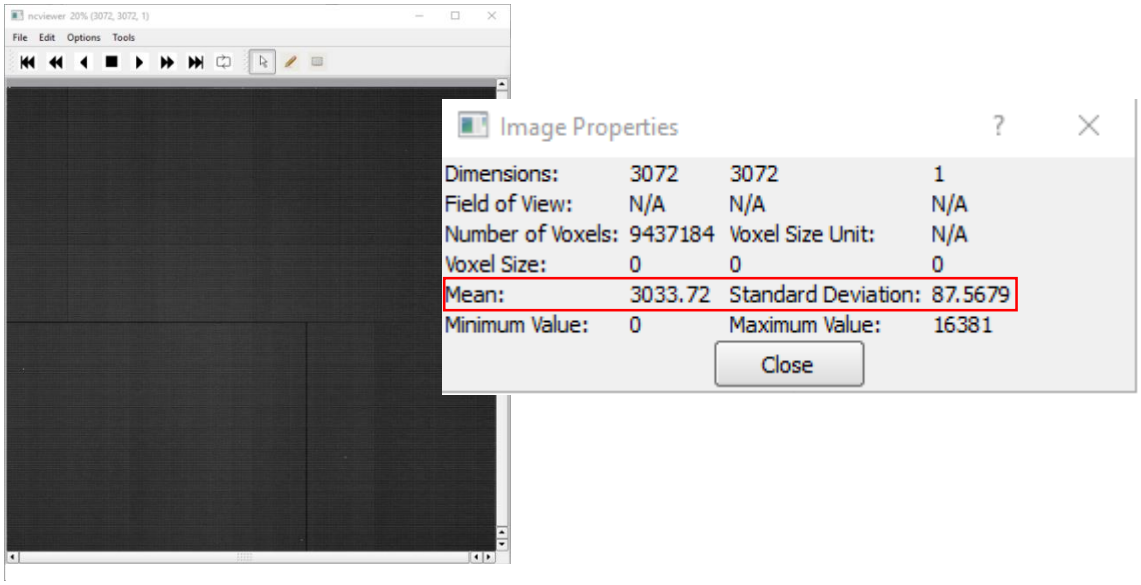

Figure 30: Offset calibration file from detector PaxScan 4343CB

4.1.4 Gain calibration

The impact of non-uniform X-ray intensity distribution on the detector area can be seen in Figure 31.

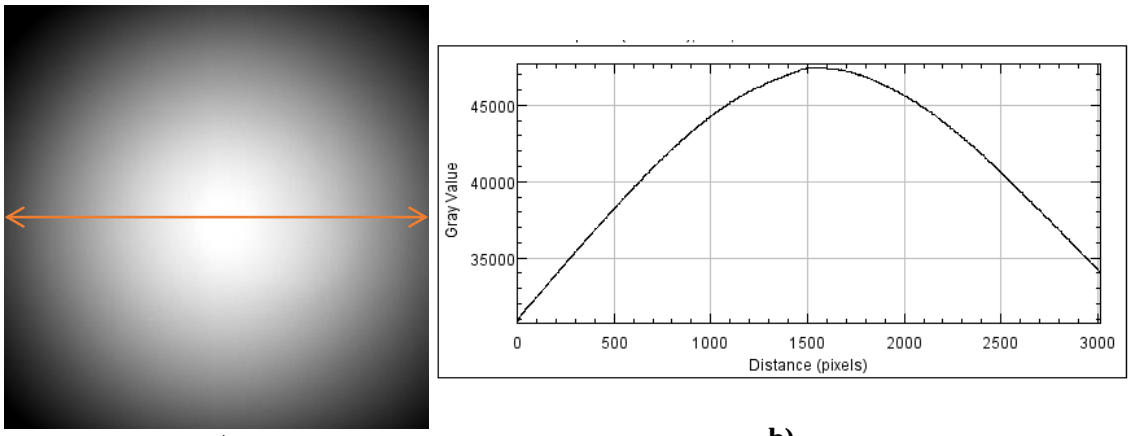

a) **b)**

Figure 31: a) Clear Field Image of non-properly calibrated detector b) Detector Intensity course across the cleat filed image

In this experiment, the detector was calibrated at 850 mm detector distance. A clear field image was taken at 330 mm detector distance. By decreasing the detector distance the ratio of edge pixel distance to center pixel distance increases. The ratio of center to edge X-ray intensity changes with second power of this ratio. The gain calibration file of the detector is in Figure 32 with its characteristic values and graph of image levels per line from the left top to the right bottom corner. The detector non-uniformity can be seen in the image as a pattern. However, the non-uniformity of the X-ray source intensity in the detector plane is more significant. Pixel levels about 11100 can be found in the image corners and pixel levels about 7900 are around the center of the image. The gain non uniformity can be expressed as the ratio standard deviation and the mean value of gain calibration image. The gain non-uniformity involves internal gain non-uniformity as well as the non-uniformity of X-ray source intensity distribution with given source - detector geometry. The gain non-uniformity is approximately 16 % in this case.

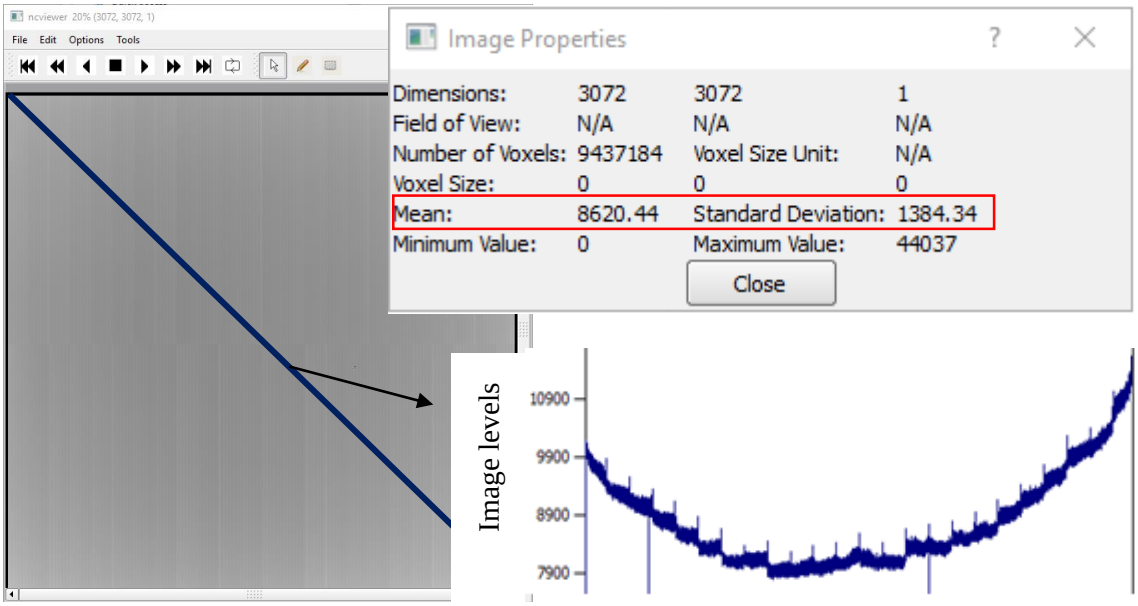

Figure 32: Gain calibration file of the detector PaxScan 4343CB at 850 mm detector distance, its mean image level and image level standard deviation and line value from left top to bottom right corner of the image

The comparison of clear filed images histograms of improperly and correctly performed gain calibrations are shown in Figure 33. It is evident that well calibrated clear field image has much narrower level spectrum than the image with improperly calibrated detector.

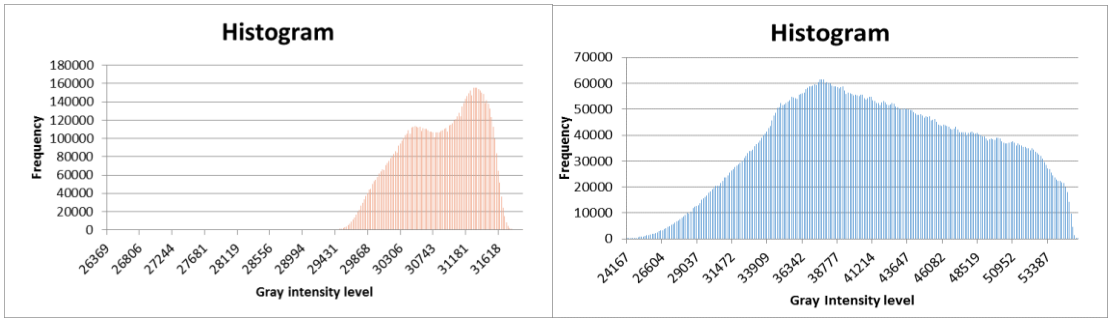

A B

Figure 33: Histograms of a clear field images taken with detector A - calibrated on the same geometry as clear field image was taken, B – calibrated on improper geometry

4.1.5 Defect pixels correction

Detector command processor contains an algorithm which compensates nonlinear responding pixels, dead (black), white pixels and noisy pixels.

Defective pixels which are not compensated can influence the artefacts that are visible in reconstructed 3D images. Defective pixels are cause of ring artifacts [39]. Reconstructed 3D slices of limestone are shown in Figure 34. The left image was scanned with a non-complete defect pixel map. On the contrary, the right picture had a precise defect pixel map.

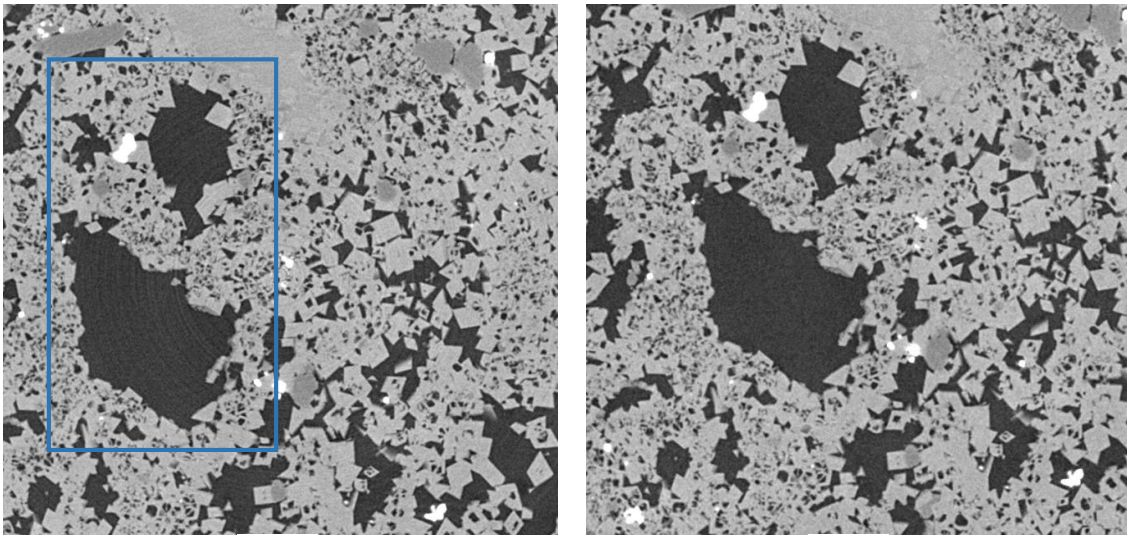

a) **b)**

Figure 34: Reconstructed data of limestone sample (a) Degeneration of the image by the ring artifacts (b) No visible ring artifact, defect map pixel correction is turned on

Defect pixel map contains bad or not correctly responding pixels. Then, those corresponding image pixels are replaced by a value which is calculated using Nearest Neighbor search algorithm. A defect pixel example is shown in Figure 29.

4.2 Influence of the detector calibrations on SNR

Offset and gain calibration detector features are important for human 2D images assessment. Typical example are medical radiographs. Similar operations are being performed in 3D reconstruction algorithms. Dark field images are used for the dark current compensation. The clear field images are used for the detector gain non-uniformity and the X-ray source non-uniformity. The compensation in the detector and in the 3D reconstruction algorithm show similar result and might not be necessary to perform both of them in series. Both of them use a digital image processing operation which introduces rounding errors and can reduce dynamic range of the input data.

Following experiment will compare SNR of 3D reconstructed slices of the same sample for various setting of the acquisition. Different accumulation numbers of acquisitions are used for particular scans. Detector image corrections were switched off in one acquisition. Purposes of the experiment are the following:

1) Proving proper correction behavior in the detector as well as the clear field and dark field functionality in 3D reconstruction algorithms. In case of non-proper functionality of any of these the significant reduction of the dynamic range and the SNR can be expected.
2) Proving the significance of performing the precise detector offset and gain calibration. Scan with a detector calibrated on scanning geometry (DD = 330mm) and some other geometry (DD = 745mm) was performed.
3) Proving the redundancy of both operations. If the scan setting with detector correction switched off gives useful results, it confirms the redundancy.

It is assumed that the detector proper gain calibration or skipping redundant correction can improve signal to noise ratio (SNR) and the dynamic range in the reconstructed images. The effect can potentially can decrease number of accumulations necessary for the projection acquisition. |Thus it can lower the total scanning time (time to data ready). The situation is demonstrated in the Figure 35. The blue line expresses our assumption, whereas the red line is the original state with an imperfect calibration or with redundant distorting calibrations.

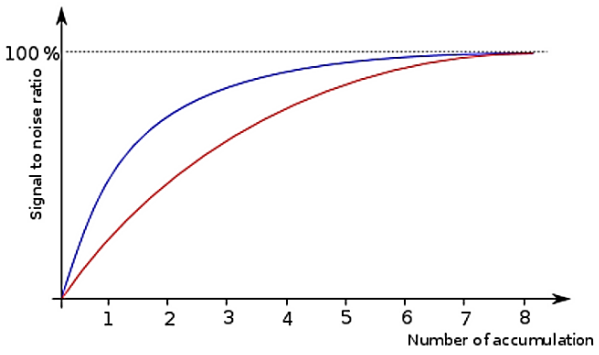

Figure 35: Estimated influence of Gain Calibration on SNR. Blue line: Performed gain calibration on the scanning distance. Red line: Standard factory gain calibration.

The basic scan parameters for the experiment are shown in table 3.

Table 3: CT scan settings for the experiment measurement

Parameter	Value
Tube Voltage	100 kV
Tube Current / Target current	60 µA / 52 µA
Focus Mode	M
Exposure Time	0.35 s
Type of scan	circular
Time of scan	~ 2 hours
Accumulations	5
Average number of counts	~ 47k

The method for SNR assessment is demonstrated in Figure 36. The SNR is measured in defined regions in the vertical 3D slice. The 3D slices and regions are the same for each scan settings. The mean value and standard deviation in the region are calculated in slices inspection tool shown in Figure 36. The mean value corresponds to the signal level and the standard deviation is taken as the noise level.

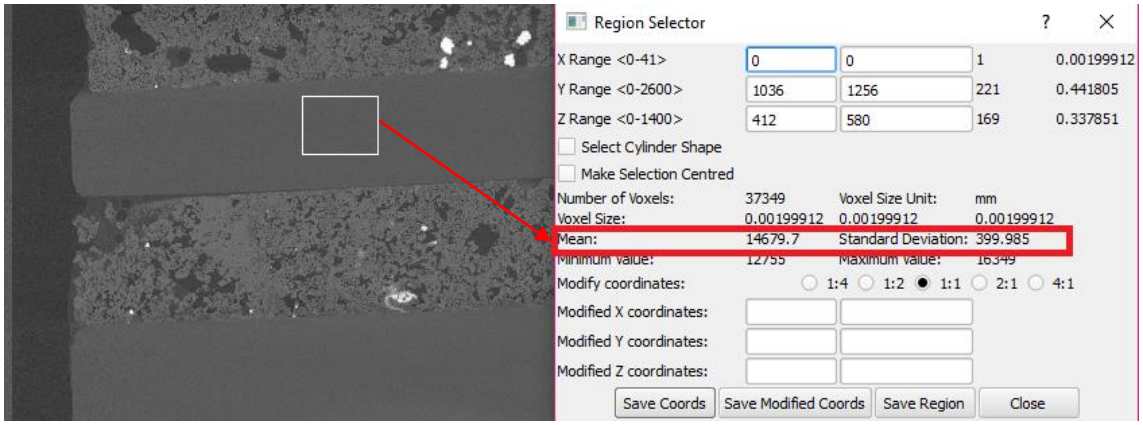

Figure 36: Selection of the region from a full NetCDF format of the reconstructed slice. Mean value and standard deviation calculation tool

The complex sample containing more materials was chosen for the experiment, see Figure 37. For the each region in the image which represents specific material the mean value of the intensity and the corresponding standard deviation were calculated. The logarithm of the ratio

of these values was multiplied by 20 to obtain the result in decibels.

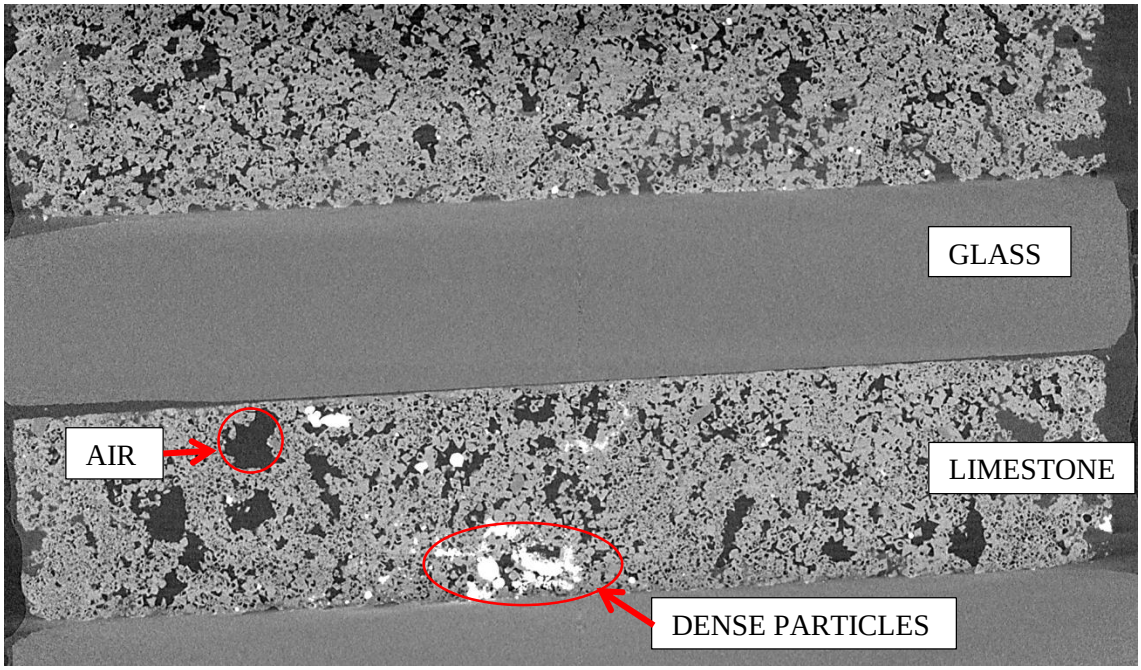

Figure 37: Reconstructed image slice of Limestone with glass, vertical cross section

4.2.1 Results of the SNR from reconstructed images

Signal to noise ratio was calculated for different materials in the scanned sample such as glass, limestone, high dense particle and air which represents the background noise. Individual scans are different in the image averaging (averaging 2 and 5) and detector calibrations.

The following Figure 38 shows bar graphs of SNR for all regions. SNR of individual scan settings is compared in particular graphs.

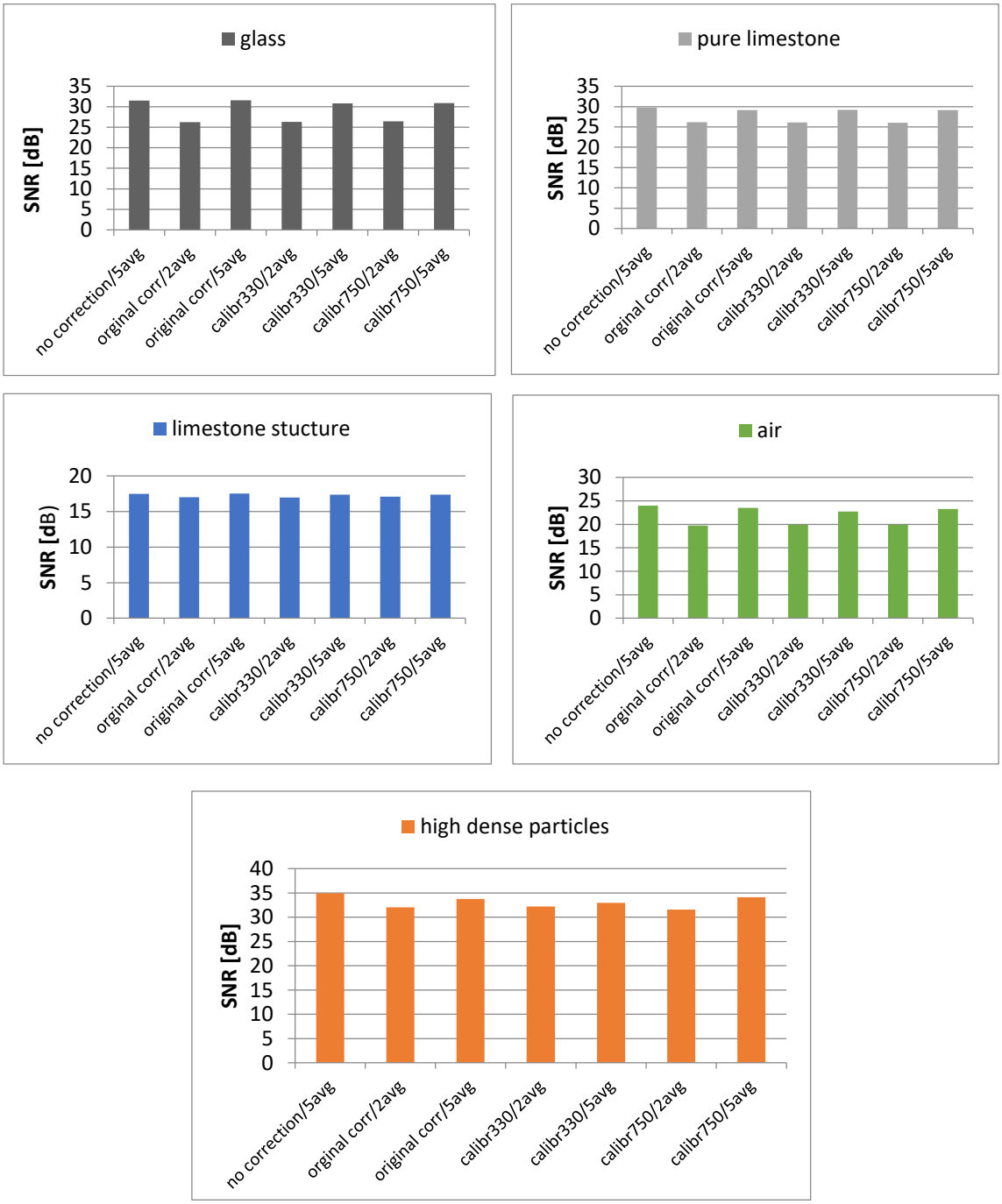

Figure 38: SNR of different slices with respect to various scan settings. Original (Factory) gain calibration (*original corr*), gain calibration performed on the DD = 330 mm (*calibr330*), gain calibration performed on the DD = 750 mm (*calibr750*), gain calibration switched off (*no correction*)

The following experiment results can be concluded based on the graphs:

- The proper function of the corrections was proved. There is no significant SNR drop

between any scans or correction settings.

- The effect of accumulation is clearly visible. Scans with two accumulations have similar SNR as well as scans with five accumulations which have better SNR but similar for each settings. The number of accumulations has the most significant impact on the SNR.
- The scan with no detector correction used has the best SNR. It means that a redundant correction causes slight additional noise and/or lower dynamic range as was expected. The cause is the redundant digital image processing operation, which involves rounding errors.
- The reconstruction of scan without the detector image corrections shows a correct image results. It confirms the assumption that one of the corrections is redundant.

4.3 Signal to Noise Ratio Measurement

4.3.1 Experiment conditions

The experiment should confirm the dependency of SNR on X-ray intensity and on number of accumulation. The goal is to verify the full dynamic range of the detector. This is achieved by exposing the detector to a dose corresponding to exposure just under the saturation. The experiment settings are shown in table 4 below

Table 4: Experiment parameters settings for the SNR measurement

Parameter	Value
Tube Voltage	90 kV
Tube Current	10 - 90 µA
Focus Mode	M
Target Current	8.7 – 60.4 µA
Exposure Time	0.25 s
Accumulations	1 - 10
Detector distance	330 mm
X-ray source temperature	21 C
Vacuum level [Pa]	2.8E-5

4.3.2 Signal to Noise Ratio calculation

There exits many ways to calculate signal to noise ratio in the literature. The experiment order is the following:

1) First of all it is necessary to subtract the Clear Field and Dark Field image and calculate the mean contrast (signal) from the subtracted images. The difference of CF and DF is the strongest signal that can be obtained from the image.
2) Blur the Clear field image and subtract the Clear Field image from the blurred one. The noise signal is obtained by this operation
3) Calculate the standard deviation of the subtracted image from the previous step
4) Divide the mean contrast by the standard deviation of subtracted Clear Field images.
5) The result is one number which corresponds to the signal and noise transfer from the input to the output.

Specialized toolbox can be used in some software environment (Matlab, Python, ...) for other image processing operations.

4.3.3 Results of SNR measurement

The dependence of the SNR on X-ray dose (corresponds to the tube current) can be seen in Figure 39. The parameter of individual curves is the number of accumulations. The experiment result is the following:

- Considering unlimited dose in microCT application for abiotic objects is suitable to set the X-ray dose on level just under the detector saturation to get the highest SNR.
- Also, it is not beneficial to use the number of accumulations higher than 4 or 5. The SNR has small improvement with higher number of them.

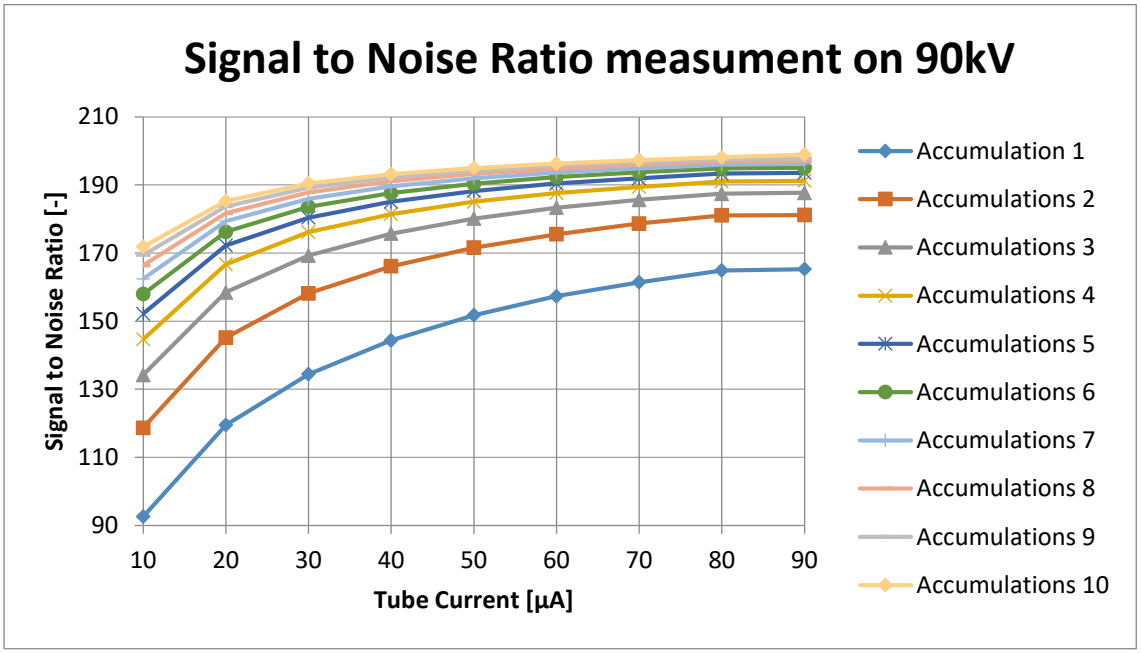

Figure 39: Dependence on a number of accumulations of signal to noise ratio

4.3.4 Image contrast measurement

The image contrast measurement in dependence on X-ray dose is in Figure 40. The curves parameters is the number of accumulations. The experiment confirmed the linear dependence of the image contrast. The number of accumulations can be understood as a multiplication of dynamic range of the image.

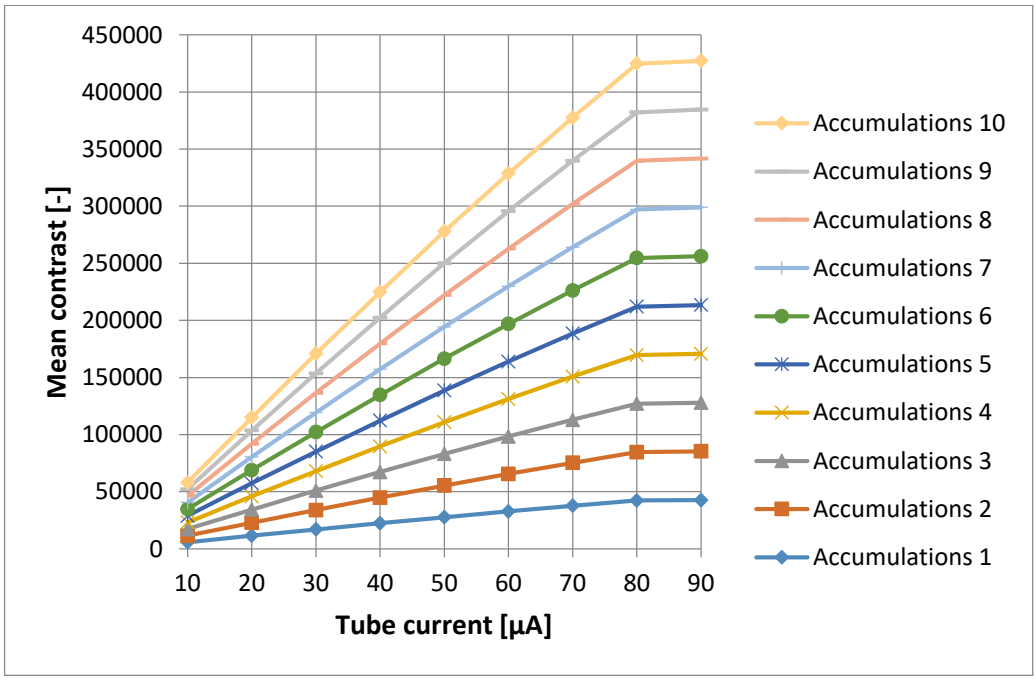

Figure 40: Influence of the Tube current on the mean contrast in the image

4.4 Dynamic Range calculation

The maximum achievable dynamic range could be given by the A/D converter bit width in case of the ideal conversion chain. The number of levels is 65 535 for a 16-bits AD converter – the PaxScan 4343CB detector in our case. The theoretical dynamic range is 96dB calculated according to the equation 3.1. However, the number of levels is reduced by non-idealities of conversion chain as explained in chapter 2.3.

The reduction of level numbers can be recalculated using the offset and gain calibration files. The Y_1 value (in Figure 22) was found as a sum of the mean and standard deviation values obtained from the offset calibration file. The AD converter level number is lowered by this value for dynamic range calculation.

The detector gain non uniformity and the X-ray source non-uniformity involves the other level number lowering. The standard deviation of gain calibration file is about 16%. It means that full ADC level numbers (65 535) lowered by Y_1 (3 122) value and multiplied by uniform gain (1 - 0.16) give a real number of ADC values (52 425). The corresponding dynamic range value in dB is 94.4.

4.5 Contrast Transfer Function

The contrast is defined as a difference between the lightest and darkest signal in the image. The contrast is the contrast dependence on spatial frequency. The variable spatial frequency phantom was used for the CTF measurement. The CTF depends on the contrast peak to peak value on spatial frequency. Basically, the CTF describes the behavior of the scintillation layer and pixelization.

The gauge shape is in Figure 41. The test pattern was placed directly on the detector and the image was acquired with following parameters:

Table 5: Parameters settings for the CTF measurement on the detector distance 330 mm

Parameter	Value
Tube Voltage	90 kV
Tube Current	75 µA
Focus Mode	M
Target Current	60.4 µA
Exposure Time	0.25 s
Accumulations	100

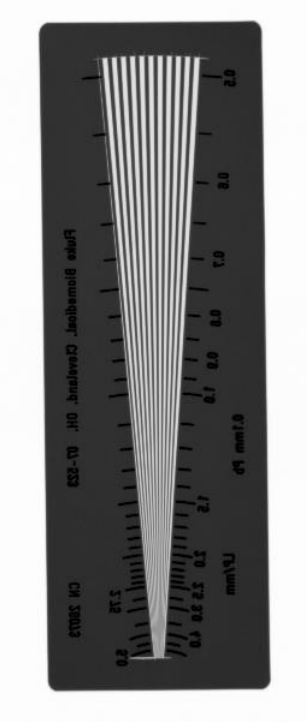

Figure 41: X-ray image of a line pair gauge

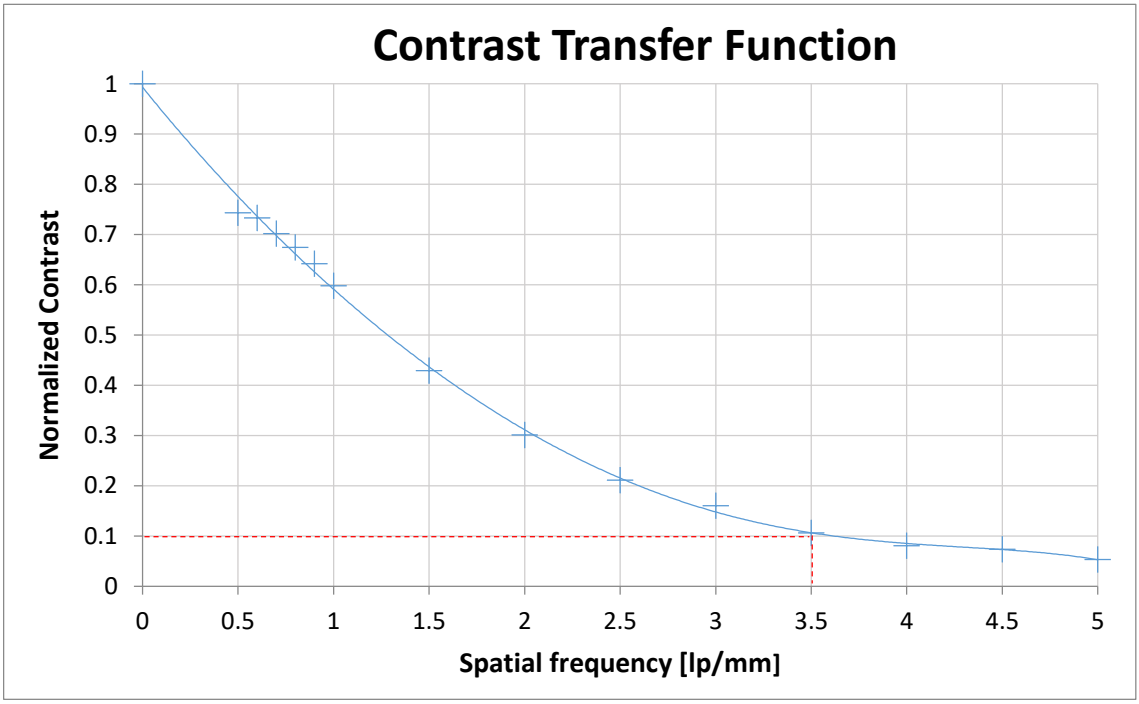

Figure 42: Contrast Transfer Function

The detector resolution is defined at the level of 10% of the CTF. The limiting resolution is about 3.5 lp/mm according to the CTF measured in Figure 42. The catalogue limit resolution for PaxScan 4343CB detector is 3.6 lp/mm [37]. The limiting resolution is theoretically calculated

according to the following equation:

$$R_{max} = \frac{1}{2 * PS} \qquad [\mathrm{lp/mm}] \tag{4.1}$$

where R_{max} is the maximum resolution and PS is the pixel size in millimeters.

This means that the limiting resolution for a detector with a pixel size of 0.139 mm is 3.597 lp/mm.

4.6 Modulation Transfer Function measurement

The Edge Method was used for Modulation Transfer Function (MTF) calculation. This method can be known also as an Edge Spread Function (ESF). The MTF describes contrast transferred in dependence on spatial frequency. This is another method for the imaging device resolution evaluation. The MTF calculation was done using the program – *ImageJ* [49] with a special COQ plugin which is described in more detail in 4.6.1.

Table 7 shows settings of the system for the MTF measurement.

Table 6: System settings for the MTF measurement

Parameter	Value
Tube Voltage	90 kV
Tube Current	80 µA
Focus Mode	M
Target Current	60 µA
Exposure Time	0.25 s
Accumulations	0
Average number of counts	~ 57k
Detector distance	330 mm

The edge image was obtained by projecting a steel ruler attached on the detector. The projection can be seen in Figure 43. Placing the ruler directly on the detector eliminates edge spreading by finite spot size.

A randomly selected part of the vertical edge was marked in the *ImageJ* software and MTF was calculated using a COQ plugin [49].

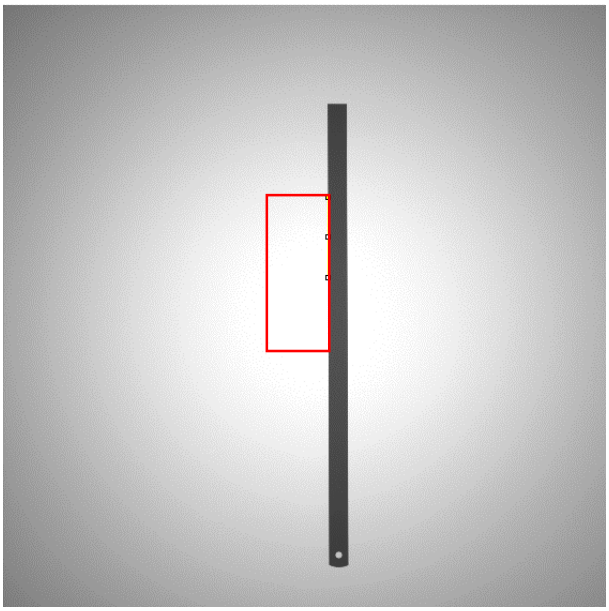

Figure 43: Iron ruler with the Edge method selection from the image, red rectangle highlights the edge selection in ImageJ COQ plugin

Measured MTF is plotted in Figure 44. The value of 54% for 1 lp/mm is stated in the detector catalogue. The value obtained from the graph is 60% for 1 lp/mm.

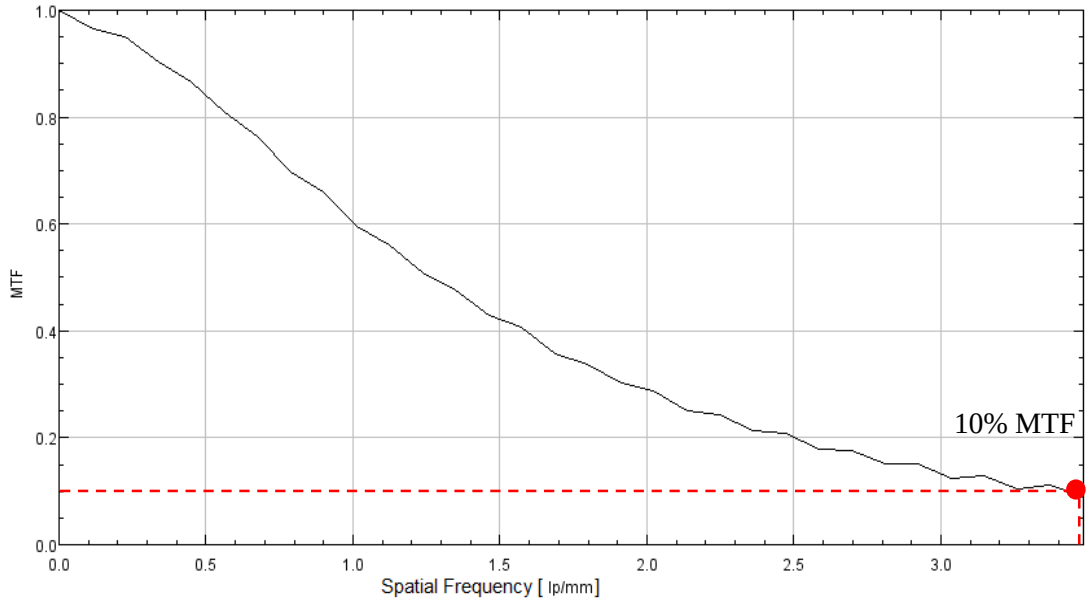

Figure 44: Measured Modulation Transfer Function

Vertical and horizontal MTF measurement have very similar results. The spatial resolution is defined as 10% of the MTF. The spatial resolution equal to 3.5 lp/mm was obtained according to our measurement [44].

4.6.1 ImageJ - COQ plugin

ImageJ is an open source image processing tool which contains many selection and drawing tools and also a number of plugins, including COQ.

COQ plugin was developed for image quality checks and measuring physical parameters such as Modulation Transfer Function (MTF), Noise Power Spectra (NPS) and Detective Quantum Efficiency (DQE) [51]. Graphical user interface is shown in Figure 45.

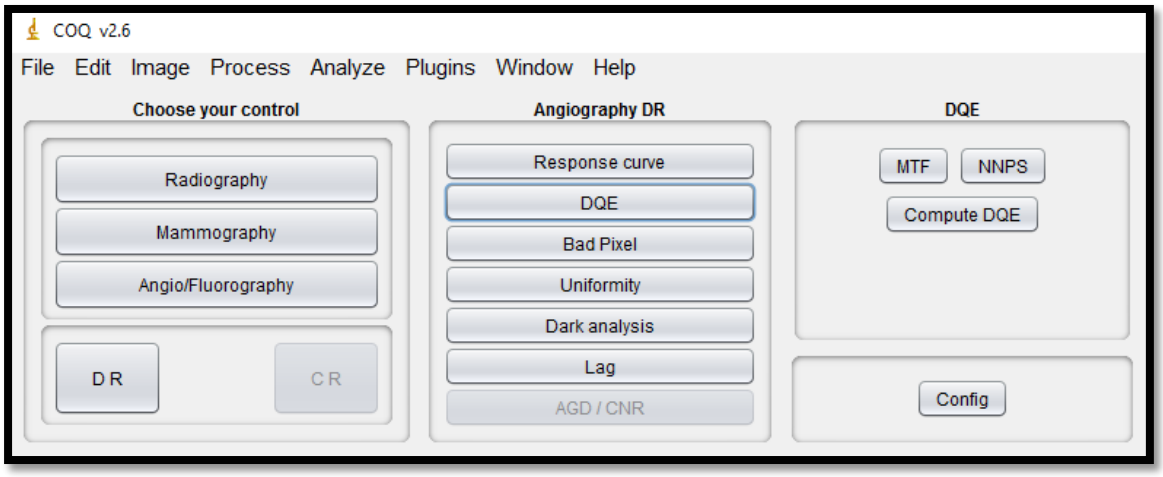

Figure 45: ImageJ - user interface of the COQ plugin

4.7 Noise Power Spectrum measurement

The Noise Power Spectrum (NPS) is important metric which describes noise variance in an image in function of the spatial frequency. Basically, the normalized NPS is a sum of different types of noise which affects the detector [6].

For the 2D calculation of a horizontal and vertical NPS 2 Clear Field images were acquired. They are first subtracted and then Fourier Transform is applied. Figure 46 shows a noise spectrum with highlighted 1-D horizontal and vertical NPS.

The results of NPS were performed with ImageJ plugin, see Figure 47.

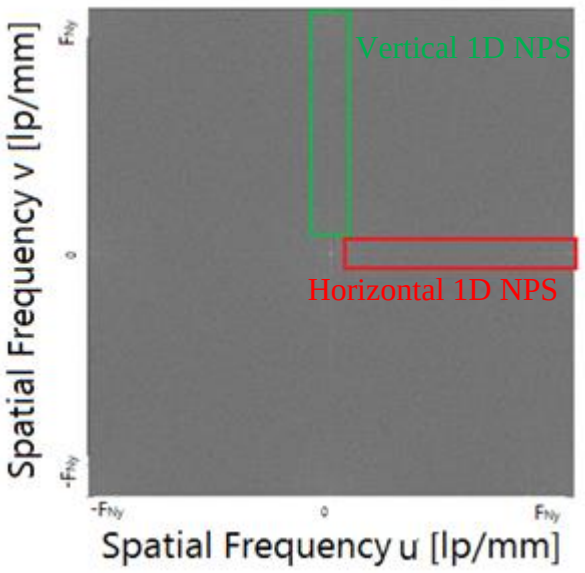

Figure 46: 2D-NPS with vertical and horizontal 1-D NPS [35]

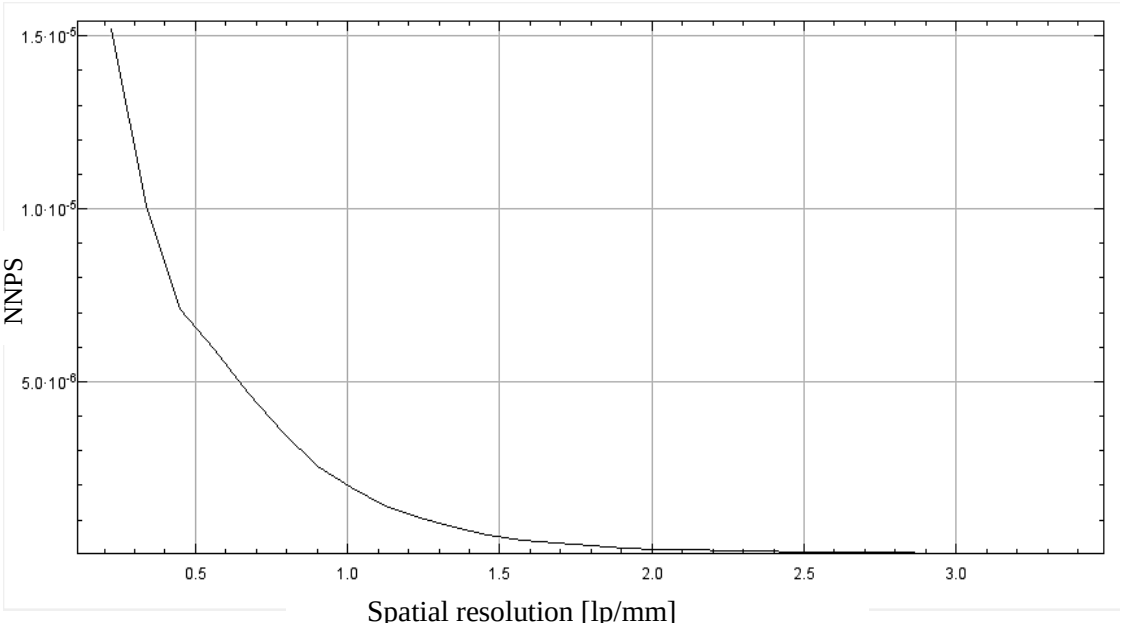

Figure 47: NNPS as a function of the Spatial Frequency

4.8 DQE – Detective Quantum Efficiency

DQE describes detector sensitivity. Higher DQE means higher resolution and contrast. DQE can be defined as a ratio of SNR on the output to the SNR on the input as a function of the spatial resolution.

For the DQE calculation the knowledge of the Modulation Transfer Function (MTF),

the Noise Power Spectrum (NPS) and also X-ray photon flux is required. DQE calculation according to the standard IEC 62220-1-3 [38, 47] is:

$$DQE(f) = \frac{MTF^2(f)}{q * NPS(q,f)}, \tag{4.2}$$

where *MTF* is Modulation Transfer Function determined according to the chapter 4.6, *NPS* is Noise Power Spectrum of the radiation filed in mm^2, u is a spatial frequency and q is a variable which is calculated as:

$$q = Ka * SNR_{in}^2 \tag{4.3}$$

Where *Ka* is the Air Kerma in μGy and SNR_{in} is defined as a signal to noise ratio per air kerma which is given by the International Electrotechnical Commission (IEC). [38]

The calculation was performed with the ImageJ plugin and results of the DQE measurement is plotted in Figure 48.

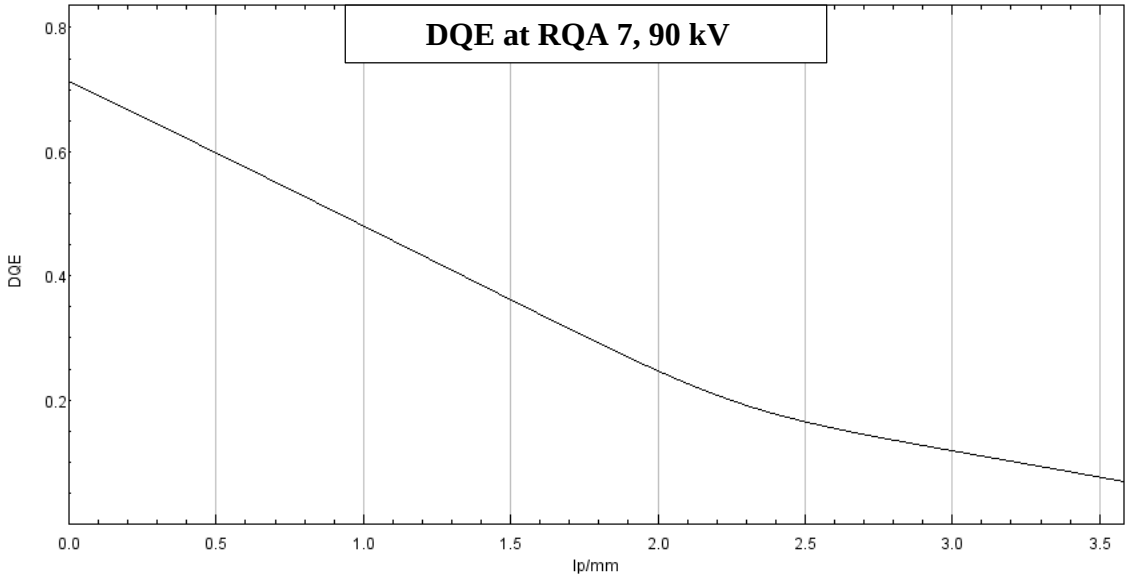

Figure 48: DQE of the PaxScan 4343CB measured using ImageJ software

4.9 FWHM method measurement

Standard edge degradation evaluation methods are the Full Width at Half Maximum or the 35 – 65 % edge level width. The second one is being used as resolution criteria in Thermo Fisher Scientific (Formerly FEI).

The detector blur is given by a pixel size in comparison with the source, where the blurriness is dependent on the magnification and the focal spot size.

For this experiment an aluminum filter which is placed on the detector surface was chosen. For the edge profile calculation the internal Python script was used. An Aluminum filter

was placed on the detector and a clear field image was taken. Figure 51 shows the picture thresholding before the edges are averaged.

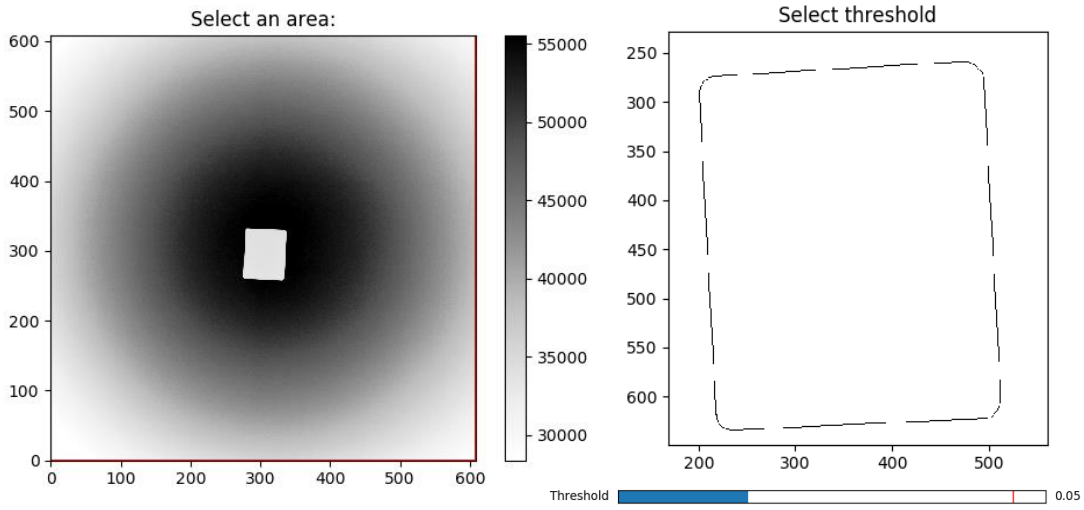

Figure 49: a) Clear Field image with placed aluminum filter on the detector b) Edges detection of the aluminum filter

The algorithm description:

1) The "*Canny edge detection*" method detects edges in the image
2) Collecting and averaging the multiple edge profiles
3) Searching the Gaussian function parameters which approximate the edge profile
4) Calculation of the edge profile derivation and measuring the FWHM
5) Comparison between the derivation of edge profiles

Detector blur ideally corresponds to the detector pixel pitch. A Varian 4343CB detector pixel pitch is 139 µm. Measurement of the detector blurring with a metal sheet is useful due to the comparability between detectors with the different pixel size.

The result of the Full Width at Half Maximum (FWHM) measurement is around 2.65 pixels which is roughly 368 µm. The result of the 35 – 65% measurement of the edge width is equal to 0.86 pixels. It is not possible to distinguish details smaller than one pixel size. Presented results are inaccurate due to the significant influence of the detector pixelization. Figure 50 shows an averaged edge profile (a), derivation of the profile (b) and auto-correlation of the derived edge profile (c).

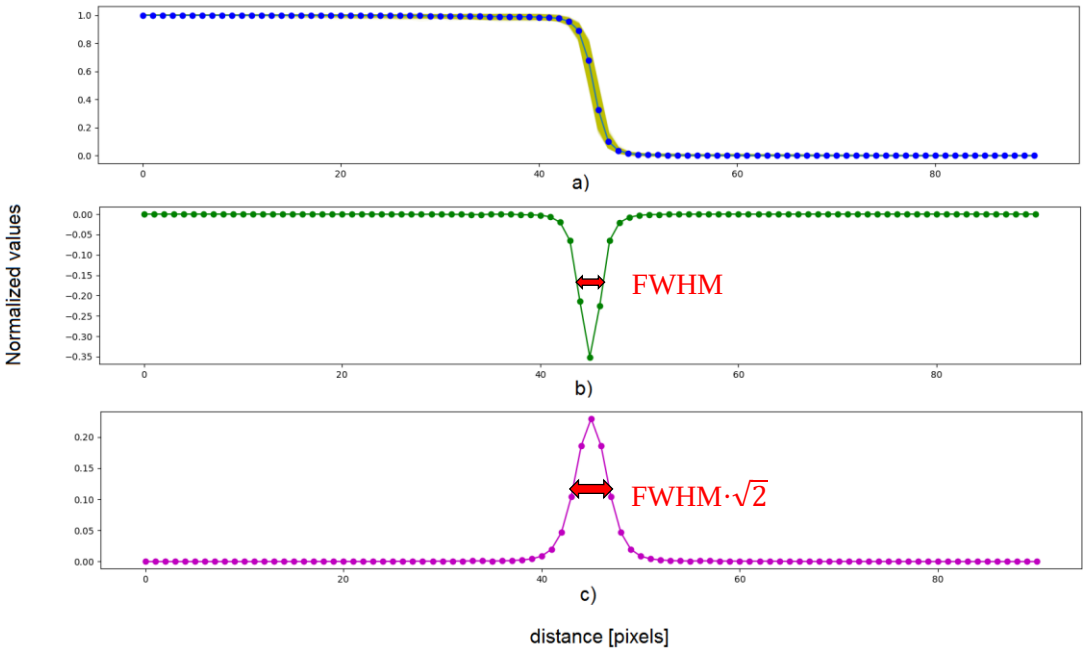

Figure 50: a) Edge profile b) Derivation of the edge profile c) Autocorrelation of the derived edge profile

Autocorrelation of the edge profile is used for the FWHM recalculation. According to the theory, Gaussian autocorrelation gives also a Gaussian but the broadening factor is $\sqrt{2}$ [40, 41].

5 MARKET RESEARCH

The following key detector features are demanded for the microCT scanner application with geometric magnification principle:

- The pixel pitch small as possible. The pixel pitch is essential parameter for detector spatial resolution. The smaller pixel pitch allows using smaller detector distances for the same resolution in the scanner configuration. The spot size has impact on the resolution as well and decreases with the decreasing detector distance.
- DQE as high as possible. The high detective quantum efficiency allows using short exposure times and performs scans quickly or allows using high resolution scans on high detector distances.
- Low noise and high dynamic range are basic requirements in any imaging system.
- The binning features are required
- Pixel array size about 3k by 3k
- The sufficient frame rate, especially in case of lower dynamic range. Smaller dynamic range detector has, higher number of accumulation is required to keep the same scanning time.
- The price is also important, however it is not the subject of this thesis.

There are no detectors dedicated to micro CT applications on the market. The most known X-ray detectors manufacturers are the following: Varex Imaging (formerly Varian), Perkin Elmer (now is also under Varex Imaging), Hamamatsu, GE, Teledyne DALSA.

Finally, the market research was done with regard to the requirements defined in the previous chapter.

Present technologies allow pixel pitch about 50 μm in detectors with other acceptable parameters for micro-CT. Selected candidates are compared in table 7. Data were obtained from catalogues [37, 45, 46]. It is clear, that the best resolution is achievable with CsI scintillator detectors due to their optical micro channel structure.

The transition to the CMOS technology would bring many benefits such as the readout speed improvement, which allows increasing a number of accumulated projections with preserving / reducing of the scanning time. PerkinElmer's detector DEXELA 2923 can be provided also with CCD/CMOS.

Table 7: Overview of different X-ray detectors and their properties

	Teledyne DALSA *Xineos 2329*	**Teledyne DALSA** *Xineos-3030HR*	**PerkinElmer** *DEXELA 2923*	**PerkinElmer** *XRD 3025*	**Varian** *PaxScan 4343*
Scintillator material	CsI	CsI	CsI	CsI	CsI
Pixel pitch [µm]	49.5	99	74.8	100	139
Binning	2x2	2x2	4x4	2x2	4x4
Chip type	CMOS	CMOS	CMOS	CMOS	CCD
Resolution	4608x5888	2994x2997	3888x3072	3004x2508	3072x3072
Max. fps	8	31	3.6 / 26	5.5	4
MTF @1lp/mm	90	58	-	80	54
DQE(0)	70	66	70	-	74
Dynamic Range	73	75	68	82	94
ADC conversion	16	14	14	16	16

CONCLUSSION

This diploma thesis deals with X-ray detectors for micro CT application. The goal of the thesis was definitions of detector parameters impact on micro-CT imaging device construction and output image quality in a 3D domain. In the next step we can define right detector parameters for micro CT scanner taking realizable detector parameters into account.

The first chapter is an introduction. CT imaging essentials are described in the second chapter. The individual parts of micro-CT scanners and its basic dependencies are defined. The third chapter is focused on detector parameters definition. Detector parameters are divided into resolution, noise, efficiency and timing categories. Parameters measurement methods are described in the chapter 3. The experimental part of the thesis is described in the fourth chapter. Parameters of the detector PaxScan 4343CB from Varex Imaging company was experimentally measured and proved. The fifth chapter is a market research. Few detector models were selected according to specified criteria for following consideration.

By the main resolution characteristic the Modulation Transfer Function (MTF) and Contrast transfer Function (CTF) the limit resolution 3.5 lp/mm was found. The result is in a good correlation with the theoretical resolution of 3.6 lp/mm. Assuming the Gaussian blurring, the MTF and the CTF measurement are equivalent.

By the particular detector measurement was found out following parameters. Calculated DQE value of 0.72 closely corresponds to the value of 0.74 declared in the product description document. As well the calculated and declared values of dynamic range of 94.0 dB and 94.4 dB respectively closely corresponds.

Used X-ray measuring methods were designed and selected to enable the objective comparison of a different detector models.

Benefits of this work are as follows:

- Described definition for the theoretical resolution of a micro-CT scanner based on the geometry and considering the spot size.
- Dynamic range was assessed for the whole conversion chain – X-ray source, detector in given geometry with respect to the real detector properties, offset and gain non-uniformity.
- Propriety implementation of detector and reconstruction corrections were verified. Also the redundancy of both corrections for 3D reconstruction was proved.

In the end, market research was conducted and PerkinElmer (now Varex Imaging) detector seems to be a suitable candidate based on specified requirements. Thus, a loan of PerkinElmer detector has been arranged for the test purposes.

REFERENCES

[1] B-Cube, *Micro-Computed Tomography*. [online]. Copyright © 2012 [cit. 2016-12-01]. Dostupné z: http://www.b-cube.ch/index.php?option=com_content&view=article&id=21&Itemid=19

[2] ŽIŽKA, Jan. Iterative reconstruction of CT image – a revolutionary milestone in computed tomography? *Ces Radiol* [online]. 2011, **65**(3), 169-176 [cit. 2016-12-02]. Dostupné z: http://www.cesradiol.cz/dwnld/CesRad_1103_169_176.pdf

[3] CORMACK, Am. *Representation of a function by its line integrals with some radiological applications*. J Appl Phys 1963; 34: 2722–2727.

[4] WANG, G. YU H, DE MAN B. *An outlook on X-ray CT research and development*. Med Phys 2008; 35: 1051–1064.

[5] EWERT, Uwe. *UPHEAVAL IN INDUSTRIAL RADIOLOGY*. 8th ECNDT. Barcelona, 2002. [cit. 2016-11-18]. Dostupné také z: http://www.ndt.net/article/ecndt02/414/414.htm

[6] TABAKOV, Slavik. *Digital Radiography Image Parameters SNR, MTF, NPS, NEQ, DQE*. College on Medical Physics. Digital Imaging Science and Technology to Enhance Healthcare in the Dev. King's College London, 2010. [cit. 2016-11-12]. Dostupné také z: http://indico.ictp.it/event/a09166/session/23/contribution/15/material/0/0.pdf

[7] ULLMANN, Vojtech. *Astro Nukl Fyzika*: [online]. [cit. 2016-12-08]. Dostupné z: http://astronuklfyzika.cz/

[8] DRASTICH, A.: *Medical Imaging Systems*. Skriptum FEI VUT v Brně pro zahraniční studenty. 2000 (EN)

[9] BRUKER. *Analysis of bone by micro - CT*: General information [online]. [cit. 2016-12-08]. Dostupné z: http://umanitoba.ca/faculties/health_sciences/medicine/units/cacs/sam/media/MN001_Bone_microCT_analysis_general.pdf

[10] ULLMANN, Vojtěch. *Jaderná a radiační fyzika*. Ostrava: Ostravská univerzita v Ostravě, Fakulta zdravotnických studií, 2009. ISBN 978-80-7368-669-7.

[11] JANEČEK, Ivan. *Atomová a jaderná fyzika*. Ostrava: Ostravská univerzita, 2003. Systém celoživotního vzdělávání Moravskoslezska. ISBN 80-7042-882-1.

[12] HALLIDAY, David, Robert RESNICK a Jearl WALKER. *Fyzika: vysokoškolská učebnice obecné fyziky*. Brno: Vutium, c2000. ISBN 80-214-1868-0

[13] BROOKS R. A., DICHIRO G., *Beam Hardening in X-Ray Reconstructive Tomography*, Phys. Med. Biol. 21(3):390–398 (1976)

[14] RITMAN EL. 2004. *Micro-Computed Tomography-Current Status and Developments*. Annual Review of Biomedical Engineering 6:

[15] ABDALLA, Munir A. *Pixel detectors and electronics for high energy radiation imaging*. Kista, Sweden, 2001. Ph. D. thesis. The Royal Institute of Technology Department of Electronics.

[16] GREGOR, T. KOCHOVA, P. Correlating Micro-CT Imaging with Quantitative Histology. Injury and Skeletal Biomechanics. InTech, 2012.

[17] BARRET, J.F. KEAT, N. (2004) *Artifacts in CT: Recognition and avoidance. Radiographics*, 24, 1679-1691. DOI:10.1148/rg.246045065

[18] DAVIS, G. R. a J. C. ELLIOTT. *Artefacts in X-ray microtomography of materials. Materials Science and Technology*. Maney Publishing, 2006, **22**(9). DOI: 10.1179/174328406X114117.

[19] *Micro-CT* [online]. [cit. 2016-12-21]. Dostupné z: http://acidoc.lifewatchgreece.eu/?q=node/20.

[20] Special Imaging Techniques. SMITH, Steven W. *The Scientist and Engineer's Guide to Digital Signal Processing* [online]. California Technical Publishing, 2011 [cit. 2016-12-21]. Dostupné z: http://www.dspguide.com/ch25/1.htm

[21] Signal-to-Noise-Ratio. *Scientific Volume Imaging B.V* [online]. [cit. 2016-12-22]. Dostupné z: https://svi.nl/SignalToNoiseRatio

[22] MIKULKA, J. Segmentační metody ve zpracování biomedicínských obrazů. Brno: Vysoké učení technické v Brně, Fakulta elektrotechniky a komunikačních technologií, 2011. 112 s. Vedoucí disertační práce: prof. Ing. Eva Gescheidtová, CSc.

[23] Technologické zajímavosti RTG přístrojů Toshiba. In: *Audio Scan* [online]. [cit. 2016-12-23]. Dostupné z: http://www.audioscan.cz/audioscan/rtg-technologicke-zajimavosti.html

[24] ENZHUO, QUAN. *Imaging Properties of a Rotation-free, Arrayed-source Micro-computed Tomography System*. ProQuest, 2009. Dissertation. Vedoucí práce Prof. David S. Lalush.

[25] BAKER, D. R. a L. MANCINI. An introduction to the application of X-ray microtomography to the three-dimensional study of igneous rocks. *LITHOS*. Elsevier B.V., 2012, (148), 262–276.

[26] HAMAMATSU. *X-ray detectors* [online]. , 21 [cit. 2016-12-31]. Dostupné z: https://www.hamamatsu.com/resources/pdf/ssd/e09_handbook_xray_detectors.pdf

[27] PAWLEY, J. B. *Handbook of Biological Confocal Microscopy*. Third edition. Springer, 2006. ISBN 978-0-387-25921-2.

[28] PONCHUT, Cyril. Characterization of X-ray area detectors for synchrotron beamlines. *Journal of synchrotron radiation* [online]. European Synchrotron Radiation Facility, Grenoble, France: International Union of Crystallography, 2006 [cit. 2017-01-03]. DOI: 0909-0495. Dostupné z: http://xrm.phys.northwestern.edu/research/pdf_papers/2006/ponchut_jsr_2006.pdf

[29] STAUDE, Andreas a Jürgen GOEBBELS. Determining the Spatial Resolution in Computed Tomography – Comparison of MTF and Line-Pair Structures. *International Symposium on Digital Industrial Radiology and Computed Tomography* [online]. BAM Bundesanstalt für Mate rialforschung und -prüfung, Berlin, (4.1) [cit. 2017-01-03]. Dostupné z: http://www.dir2011.com/Portals/dir2011/BB/tu41.pdf

[30] PAULUS MJ, GLEASON SS, KENNEL SJ, HUNSICKER PR, JOHNSON DK. *High Resolution X-ray Computed Tomography: An Emerging Tool for Small Animal Cancer*

Research. Neoplasia (New York, NY). 2000;2(1-2):62-70

[31] TURCHETTA, Renato, Kenneth R. SPRING a Michael W. DAVIDSON. Introduction to CMOS Image Sensors. In: *Microscopy resource center* [online]. Olympus, 2012 [cit. 2017-01-03]. Dostupné z: http://olympus.magnet.fsu.edu/primer/digitalimaging/cmosimagesensors.html

[32] STUART, R. S. MicroComputed Tomography: Methodology and Applications, Boca Raton, 2009.

[33] MESSTECHNIK, W. X-Ray Tomography in Industrial Metrology, ISBN 978-3-86236-045-1, 2nd ed., 2012

[34] ALLBECK, C. NELDAM, T. L. Application of high resolution synchrotron micro-CT radiation in dental implant osseo integration, *Journal of Cranio-Maxillofacial Surgery*, Volume 43, Issue 5, June 2015, Pages 682-687, ISSN 1010-5182.

[35] KONSTANTINIDIS, Anastasios C. *Evaluation of digital X-ray detectors for medical imaging applications*. London, 2011. University College London.

[36] HALÁMEK, J, M KASAL a I VIŠČOR. *Dynamic range and acquisition system*. *MEASUREMENT SCIENCE REVIEW* [online]. Institute of Scientific Instruments, AS CR, Brno, 2001, **1**(1), 1-4 [cit. 2017-01-04]. Dostupné z: http://www.measurement.sk/PAPERS/Halamek1.pdf

[37] VARIAN MEDICAL SYSTEMS. *PaxScan 4343CB Operating Instructions: Digital Image Receptor* [online]. Rev A. 2012 [cit. 2017-04-18]. Dostupné z: https://www.varian.com/sites/default/files/resource_attachments/4343CB_0.pdf

[38] IEC 62220-1:2003(E). International standard IEC 62220-1: Medical electrical equipment – Characteristics of digital X-ray imaging devices – Part 1: Determination of the detective quantum efficiency. GENEVA, SWITZERLAND: IEC Central Office, 2003.

[39] ELSHIEKH, E., I. I. SULIMAN a F. HABBANI. Performance evaluation of two computed radiography systems and patient dose in pelvic examination. *Radiation Protection Dosimetry* [online]. 2015, **165**(1-4), 392-396 [cit. 2017-04-18]. DOI: 10.1093/rpd/ncv125. ISSN 0144-8420. Dostupné z: https://academic.oup.com/rpd/article-lookup/doi/10.1093/rpd/ncv125

[40] RAVEN, Carsten. Numerical removal of ring artifacts in microtomography. *REVIEW OF SCIENTIFIC INSTRUMENTS* [online]. Grenoble Cedex, France, 1998, **69**(8), 1-3 [cit.2017-04-19]. Dostupné z: http://qmxmt.com/scans/dave/other/papers/xmt%20artefacts/numerical%20removal%20of%20ring%20artifacts%20in%20microtomography.pdf

[41] PULSE LENGTH MEASUREMENT [online]. Del Mar Photonics [cit. 2017-04-25]. Dostupné z: http://www.dmphotonics.com/Autocorrelator/8_PULSE_LENGTH.pdf

[42] BUSHBERG, Jerrold T. *The essential physics of medical imaging*. 2nd ed. Philadelphia: Lippincott Williams & Wilkins, c2002. ISBN 0683301187.

[43] ŠKRABAL, Pavel. *Ověření možností použití obrazových detektorů Rad-icon Imaging v radiologii* [online]. Praha, 2007 [cit. 2017-05-08]. Dostupné z: https://is.cuni.cz/webapps/zzp/download/130084586. Bakalářská práce. Univerzita Karlova v Praze, 1. Lékařská fakulta. Vedoucí práce Ing. Jiří Hozman, Ph.D.

[44] TJONG, Willy, Galateia J. KAZAKIA, Andrew J. BURGHARDT a Sharmila MAJUMDAR. The effect of voxel size on high-resolution peripheral computed tomography measurements of trabecular and cortical bone microstructure. Medical Physics [online]. 2012, **39**(4), 1893-1903 [cit. 2017-05-08]. DOI: 10.1118/1.3689813. ISSN 00942405. Dostupné z: https://www.ncbi.nlm.nih.gov/pubmed/22482611

[45] ZHAO, Chumin, Jerzy KANICKI, Anastasios C. KONSTANTINIDIS a Tushita PATEL. *Large area CMOS active pixel sensor x-ray imager for digital breast tomosynthesis: Analysis, modeling, and characterization*. *Medical Physics* [online]. 2015, **42**(11), 6294-6308 [cit. 2017-05-10]. DOI: 10.1118/1.4932368. ISSN 00942405. Dostupné z: http://doi.wiley.com/10.1118/1.4932368

[46] *Xineos 2329 CMOS X-Ray Flat Detector: Better Images, Lower Dose for Mammography* [online]. Teledyne DALSA [cit. 2017-05-10]. Dostupné z: https://www.teledynedalsa.com/imaging/products/x-ray/dynamic-flat/xineos/XINEOS-2329/

[47] KONSTANTINIDIS, Anastasios, Magdalena SZAFRANIEC a Robert SPELLER. The Dexela 2923 CMOS X-ray detector: A flat panel detector based on CMOS active pixel sensors for medical imaging applications. *Nuclear Instruments and Methods in Physics Research A* [online]. London: Department of Medical Physics and Bioengineering, Malet Place Engineering Building, University College London, Gower Street, London, WC1E 6BT, UK, 2012, (689), 12-21 [cit. 2017-05-10]. Dostupné z: http://www.sciencedirect.com/science/article/pii/S0168900212006730

[48] DESAI, Nikunj a Abhinav SINGH. *Practical Evaluation of Image Quality in Computed Radiographic (CR) Imaging Systems* [online]. Department of Biomedical Engineering, University of California, 1-10 [cit. 2017-05-11]. Dostupné z: http://www.moderntech.com.hk/sites/default/files/whitepaper/V06_Manuscript_0.pdf

[49] *ImageJ plugin for performing physical characterization and quality checks* [online]. In: ALMA MATER STUDIORUM - Università di Bologna: Department of physics - Medical imaging [cit. 2017-05-11]. Dostupné z: http://www.medphys.it/down_dqe.htm

[50] ZMESKAL, Johann. *Detector and detector systems for particle and nuclear physics I* [online]. In: Österreichische Akademie der Wissenschaften, 2015, s. 1-99 [cit. 2017-05-13]. ISBN VO 260 066. Dostupné z: https://www.oeaw.ac.at/fileadmin/subsites/etc/Institute/SMI/PDF/Detectors_WS2014-15_A2.pdf

[51] DONINI, Bruno, Stefano RIVETTI, Nico LANCONELLI a Marco BERTOLINI. Free software for performing physical analysis of systems for digital radiography and mammography. *Med. Phys.* [online]. 2014, **41**(5), 1-10 [cit. 2017-05-13]. Dostupné z: http://www.medphys.it/publications/MP14.pdf

[52] VARIAN MEDICAL SYSTEMS. *PaxScan 4343CB Operating Instructions: Digital Image Receptor* [online]. Rev A. 2012 [cit. 2017-04-18]. Dostupné z: https://www.varian.com/sites/default/files/resource_attachments/4030MCT_0.pdf

[53] TOLLEY, Guy a Sheng YUE. BEAM HARDENING – WHAT IS IT AND HOW TO REDUCE IT. In: *North Star Imaging Blog* [online]. UK: UK Sales and Inspection Services, 2016 [cit. 2017-05-17]. Dostupné z: http://4nsi.com/blog/2016/02/12/beam-hardening/

List of symbols and abbreviations

CT	Computed Tomography
CCD	Charged Coupled Devices
CMOS	Complementary Metal Oxide Semiconductors
FBP	Filtered back projection
DQE	Detective Quantum Efficiency
SNR	Signal to Noise Ratio
MTF	Modulation Transfer Function
LSF	Line Spread Function
ESF	Edge Spread Function
PSF	Point Spread Function
CTF	Contrast Transfer Function
FWHM	Full Width at Half Maximum
μ	Attenuation coefficient
SD	Sample distance
DD	Detector distance
SS	Spot size
NPS	Noise Power Spectrum
IR	Iterative reconstruction
CsI	Cesium Iodide
G	Gain
GOS	Gadox
NaI(Tl)	Iodide activated by thallium
DR	Dynamic range
EBL	Edwards Brown Limestone
FOP	Fiber Optic Plates
CF	Clear Field
DF	Dark Field
ADC	Analog Digital Converter